

A model for plasma modification of polypropylene using atmospheric pressure discharges

Rajesh Dorai^{1,3} and Mark J Kushner^{2,4}

¹ University of Illinois, Department of Chemical Engineering, 1406, West Green Street, Urbana, IL 61801, USA

² University of Illinois, Department of Electrical and Computer Engineering, 1406, West Green Street, Urbana, IL 61801, USA

E-mail: mjk@uiuc.edu

Received 14 November 2002

Published 26 February 2003

Online at stacks.iop.org/JPhysD/36/666

Abstract

Atmospheric pressure plasmas are commonly used to improve the wetting and adhesion properties of polymers. In spite of their use, the mechanisms for achieving these properties are unclear. In this regard, we report on a computational investigation of the gas phase and surface kinetics during humid-air corona treatment of polypropylene (PP) and the resulting modification of its surface properties while varying energy deposition, relative humidity (RH), web speed, and gas temperature. Using results from a global plasma chemistry model validated against experiments, we found that increasing energy deposition increased the densities of alcohol, carbonyl, acid, and peroxy radicals on the PP surface. In doing so, significant amounts of gas phase O₃ and N_xO_y are produced. Increasing the RH increased the production of peroxy and acid groups, while decreasing those of alcohol and carbonyl groups. Production of O₃ decreased while that of HNO₃ increased. Increasing the temperature decreased the concentrations of alcohol, carbonyl, and acid groups on PP while those of the peroxy radicals increased. For a given energy deposition, higher web speeds resulted in decreased concentrations of alcohols, peroxy radicals, carbonyl, and acid groups on PP.

1. Introduction

Plasmas sustained at atmospheric pressure are commonly used to improve the adhesion and printing properties of polymers [1]. In these surface treatments, only the top hundreds of angstroms of the material are modified leaving the bulk polymer largely unaffected [2]. Although low-pressure plasma processes can be used for this purpose, atmospheric pressure processes are attractive for industrial applications because of their lower cost, higher throughput, and ability to operate without vacuum systems.

A variety of polymers have been treated by plasmas, including polypropylene (PP) [3–9], polyethylene (PE) [3, 10–15], poly(tetrafluoroethylene) [16], polyimide [17, 18],

polystyrene [15], polycarbonate [19, 20]. The aim of these treatments is generally to improve the wetting and adhesion properties of the polymers. For example, Shenton *et al* [21] observed that atmospheric pressure plasma treatment of low density PE and poly(ethylene terephthalate) improved adhesion by factors of two to ten.

In general, the surface energy of untreated polymers is too small for good adhesion. For optimum adhesion, the surface energy of the polymer should be larger than that of the material to be bonded with. Similarly, for effective wetting by a liquid, the surface energy of the polymer should exceed the surface tension of the liquid. The surface energy of untreated PP is $\approx 27 \text{ mJ m}^{-2}$ [5, 22], whereas the surface tensions of typical water-based adhesives are 44–50 mJ m^{-2} and those of water-based inks are 54–56 mJ m^{-2} [23]. The surface energy depends on the liquid used for measurement, and the polar and non-polar components of the surface energy are determined by

³ Present address: Varian Semiconductor Equipment Associates, 35 Dory Road, Gloucester, MA 01930, USA.

⁴ Author to whom correspondence should be addressed.

using polar and non-polar solvents [24]. In general, plasma surface treatment can increase the overall surface energy of PP above that of these classes of adhesives and inks, thereby enabling bonding and printing. For example, in studies of atmospheric pressure plasma treatment of PP in He (containing ppm levels of O₂ and H₂O) by Massines and Gouda [5], the surface energy of PP increased from 27 mJ m⁻² to as high as 62 mJ m⁻². The increase was attributed primarily to the bonding of O atoms to the PP surface.

Plasma surface treatment of polymers primarily results in the oxidation of the surface by the generation of functional groups such as C–OH (alcohol), C–O–O–H (hydroperoxide), H–C=O (aldehyde), C=O (carbonyl), C–O–C=O (ester), C–O–O• (peroxy), H–O–C=O (acid), OC(O)O (carbonate), and NH₂ (amine). For example, following the treatment of PE by an air plasma, Foerch *et al* [11] observed the formation of ester, alcohol, carbonyl, and acid groups by x-ray photoelectron spectroscopy. Surface physicochemistry studies of air-corona-discharge-treated PP by O'Hare *et al* [25] showed the presence of alcohol, peroxide, acid, ester, carbonyl, and carbonate groups on the surface.

In addition to functionalization, other phenomena such as ablation of the polymer, chain scission, and cross-linking may occur with corona treatment [1, 26]. Clouet and Shi [10] used hexatriacontane (C₃₆H₇₄) as a proxy for high-density PE to study the gas phase products of plasma surface oxidation and ablation. They found that CO, H₂O, CO₂, and H₂ were the primary products in an oxygen rich plasma. Hansen *et al* [27] studied the effects of atomic oxygen on polymers such as PE, PP, polyimide, and polysulfide. Emission of CO₂ was observed and correlated with the ablation of the polymer at a rate directly proportional to the duration of the treatment. CO₂ plasmas have been found to result in less ablation of PP compared to O₂ plasmas [28].

The ablation of the polymer occurs through chain scissions and the formation of low molecular weight oxidized materials (LMWOMs). The volatile components of LMWOM can leave the surface [8, 29]. Under select conditions, LMWOMs have been found to agglomerate into globules at the surface due to a large difference in interfacial free energy between the underlying hydrophobic substrate and the oxygenated overlayer [30]. In studies of point-to-grid DC corona discharge treatment of PE, Takahashi *et al* [14] observed the formation of LMWOM when the energy deposition exceeded a threshold value. They also found that properties such as surface energy saturated for energies above the threshold. Strobel and Lyons [31] investigated the consequences of LMWOM produced by corona treatment of PP on its sticking properties by adhering different materials to the modified surface: a polyamide printing ink, vapour coated aluminium, a synthetic rubber pressure-sensitive adhesive, and an acrylate based pressure-sensitive adhesive. They found that the adhesion was enhanced for the ink and the acrylate based material where the LMWOM was incorporated into the adherate. When the LMWOM was not incorporated into the adherate, as in the case for the metal and the rubber-based adhesive, they found that LMWOM acts as a weak boundary layer inhibiting adhesion.

The relative concentrations of functional groups on a treated surface generally depend on the operating conditions of the plasma generator such as energy deposition and gas

composition for a given polymer being processed. These interrelations can be quite complex. In studies of N₂ microwave plasma modification of PP, Poncin-Epaillard *et al* [6] detected $\approx 2.5 \times 10^{14}$ cm⁻² of amino groups for a power deposition of 100 W. Higher concentrations of these groups were observed on PE for treatments with shorter durations (higher frequency) and powers greater than 50 W. Hansen *et al* [27] found that the rates of oxidation of branched polymers such as PP were higher compared to the relatively unbranched hydrocarbon polymers such as PE for otherwise the same operating conditions. Some systematic trends are however, clear. Oxygen plasma treatment generally increases the surface energy of polymers, whereas fluorocarbon plasma treatment generally decreases the surface energy by creating CF₂ or CF₃ functional groups thereby making the polymer more hydrophobic and chemically inert [2, 32]. Low surface energies can also be obtained by the insertion of oriented methyl groups into the polymer chain [33].

In this regard, several gases have been investigated for modifying the surface properties of PP, including He [5], CO₂ [28], N₂ [6, 22], NH₃ [34], and air [9, 22, 35]. Studies by Massines *et al* [35] on the role of gas composition in the dielectric barrier discharge (DBD) treatment of PP showed that O₂, even when present in small quantities, can significantly affect the surface chemistry and hence the level of surface transformation. When $\approx 0.2\%$ of O₂ was added to N₂, the percentage of O on the surface doubled while that of N decreased by a factor of five [35]. Meiners *et al* [36] showed that exposure of PP to an Ar plasma followed by exposure to pure acetylene gas (C₂H₂) increased the surface energy from 30 to 72 mJ m⁻². A thin polymeric film was formed on the PP surface which both increased and stabilized the surface energy. When only an air or Ar plasma was used, the surface energy reached 40 mJ m⁻².

The nature of the discharge also affects the surface properties of the polymer. Under controlled operating conditions, stable, uniform, non-filamentary or glow discharges, can be produced which are often more effective for surface modification compared to filamentary discharges [5]. Massines *et al* [5] showed that the surface energy of PP increased from 27 to 62 mJ m⁻² when using a glow (non-filamentary) atmospheric discharge, whereas with filamentary discharges, the surface energy increased to only 45 mJ m⁻². The contact angle for the glow discharge treated PP was 32° and that for the filamentary discharge treated PP was 57° (the smaller the contact angle, the larger is the wettability).

Plasma modified polymer surfaces may age, a process commonly attributed to the migration of groups on the surface after treatment, surface reorientation, and exposure to oxidizing environments [4]. Ageing depends on the type of polymer and the process conditions. For example, studies of air-corona-discharge-treatment of PP by Strobel *et al* [4] showed the effects of ageing to be minimal. The O/C ratio on the surface did not significantly change while the wettability decreased by <5% after 30 days. This change was attributed to the reorientation of surface groups. Guimond *et al* [22] showed that the increase in surface energy of PP produced by a N₂ glow discharge decreased by ageing. After treatment, the surface energy was ≈ 53 mJ m⁻². After 10 days, the surface energy stabilized to ≈ 44 mJ m⁻².

In this paper, we present results from our computational investigations on the gas phase and surface kinetics during the modification of PP in humid-air plasmas. A pseudo-homogeneous global kinetics model interfaced to a surface site balance model was developed and validated against experiments. The consequences of process variables which have experimentally been found to control the resulting surface properties [1] (energy deposition, relative humidity (RH), gas temperature, and web speed) were investigated. We found that increasing energy deposition not only increases densities of peroxy and acid groups on the PP surface, but also increases the production of gas phase byproducts such as N_xO_y and O_3 . Increasing the RH decreased the production of O_3 and increased the concentrations of peroxy and acid groups on the surface. The surface concentrations of peroxy radicals increased with RH while those of alcohol, carbonyl, and acid groups decreased. Increasing the gas temperature increased the surface concentration of peroxy radicals and decreased the concentrations of alcohol, carbonyl, and acid groups. For a given energy deposition, increasing the web speed decreased the densities of peroxy, alcohol, carbonyl, and acid groups on the PP surface.

The model used for the study, GLOBAL_KIN is described in section 2. The gas phase reaction mechanism for humid-air and the surface reaction mechanism for PP are described in sections 3 and 4. Results for plasma surface modification of PP are presented in section 5. Concluding remarks are in section 6.

2. Description of the model

A schematic of a typical corona device used for plasma surface modification is shown in figure 1(a). The device consists of a grounded electrode covered with a dielectric and a metal shoe electrode, across which tens of kilovolts sinusoidal pulses at tens of kilohertz are typically applied to produce discharges in air. These discharges are usually in the form of microstreamers which are typically tens to hundreds of micrometre in diameter, with an area density of tens to hundreds per square centimetre and durations of a few to hundreds of nanoseconds [35]. Typical web speeds are tens to hundreds of metre per minute and the polymer usually spends a maximum of a few seconds in the discharge. Energy depositions are usually 0.1 to a few joules per square centimetre. Although the plasma equipment used industrially for polymer processing are typically called corona discharges, due to the dielectrics on the electrodes and the capacitance of the polymer, the devices function as DBDs.

The model used in this study is a modified version of a homogeneous plasma chemistry simulator called GLOBAL_KIN [37]. To address the reactions on and near the polymer surface, a heterogeneous model was developed and incorporated into GLOBAL_KIN. In GLOBAL_KIN, the temporal evolution of volume-averaged species densities is modelled. Based on the user defined reaction mechanism, the rate equations for the production and consumption of species both in the gas phase and on the polymer surface are constructed. Rate constants for heavy particle reactions were calculated using Arrhenius expressions based on the gas temperature. The rate constants for electron-impact reactions

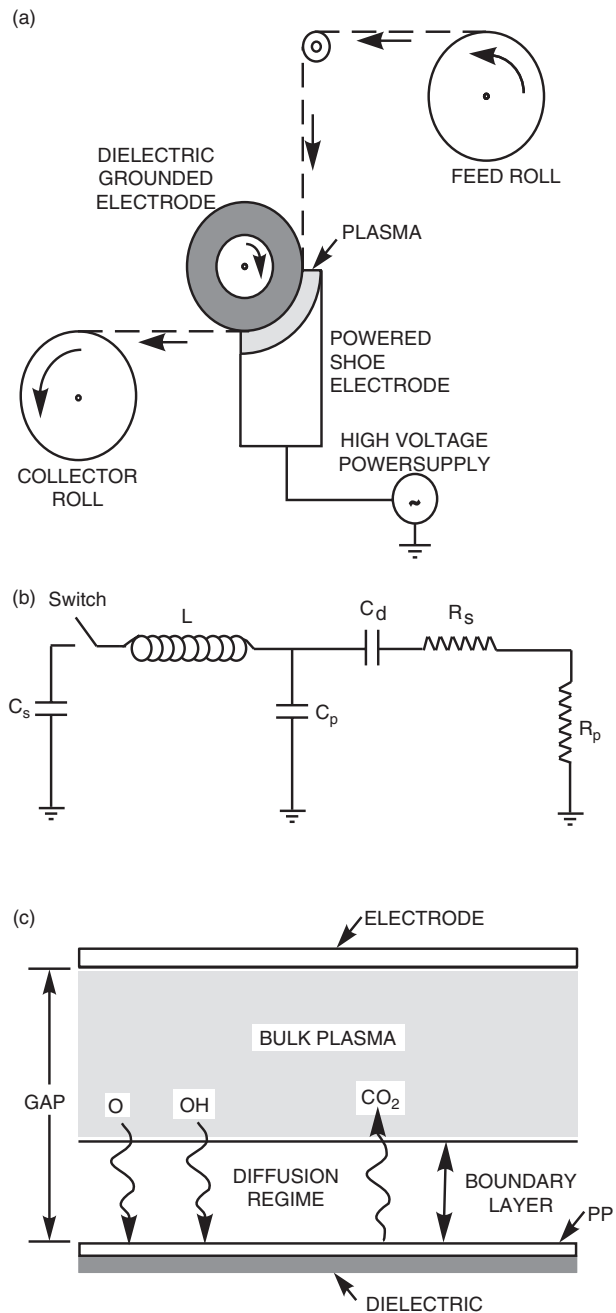


Figure 1. Model for plasma polymer surface treatment. (a) Schematic of the plasma polymer surface treatment process. A plasma is created in air by applying tens of kilovolts sinusoidal pulses at tens of kilohertz across a few millimetre gap. The polymer web traverses the plasma region at speeds of tens to a few hundreds of metres per minute. Typically, the residence time of the polymer in the plasma is at most a few seconds. (b) Discharge circuit used in the model. (c) Quasi homogeneous model for species transport to the polymer surface. Two zones above the PP surface are considered—a diffusion boundary layer and homogeneous bulk plasma. Species produced in the bulk plasma diffuse through the boundary layer, react with the polymer surface, and the products diffuse back to the bulk through the boundary layer.

were obtained as a function of electron temperature by solving the two-term spherical harmonic expansion of Boltzmann's equation for the electron energy distribution and parametrizing for several values of the reduced electric field [39].

The reaction set typically includes: electron-impact processes in the gas phase which result in ionization, dissociation, excitation, electron-ion recombination, and attachment; heavy species reactions in the gas phase that result in neutral chemistry, charge exchange, ion-ion neutralization; reactions of gas phase species with species on the surface; and reactions between surface species. The reaction mechanism involves 90 species (65 in the gas phase and 25 on the polymer surface) and nearly 400 reactions. The complete set of reactions can be found in [38].

The electron temperature is determined by the energy gained by Joule heating, and the energy dissipated in elastic and inelastic collisions,

$$\frac{d}{dt} \left(\frac{3}{2} n_e k_B T_e \right) = \vec{j} \cdot \vec{E} - \sum_i \frac{3}{2} n_e \nu_{mi} \left(\frac{2m_e}{M_i} \right) k_B (T_e - T_i) + \sum_l n_e k_l N_l \Delta \varepsilon_l. \quad (1)$$

n_e is the electron density, T_e is the electron temperature, \vec{j} and \vec{E} are the current density and the electric field in the discharge, ν_{mi} is the electron momentum transfer collision frequency with species i , m_e is the electron mass, k_B is the Boltzmann's constant, and M_i and T_i are the mass and temperature of species i . For the l th electron impact process, k_l is the reaction rate coefficient, N_l is the density of the gas phase collision partner, and $\Delta \varepsilon_l$ is the change in the electron energy.

The average gas temperature T_g is obtained by accounting for heating from elastic and inelastic collisions with electrons, enthalpy of heavy particle reactions, and heat transfer to surfaces,

$$\frac{d}{dt} (N c_p T_g) = \sum_i \frac{3}{2} n_e \nu_{mi} \left(\frac{2m_e}{M_i} \right) k_B (T_e - T_i) + \sum_j n_e k_j N_j \Delta \varepsilon_j - \sum_j \Delta H_j R_j - h_{\text{eff}} \frac{T_g - T_w}{d_{\text{gap}}}, \quad (2)$$

where N is the total gas density, c_p is the specific heat, and ΔH_j and R_j are the change in enthalpy and rate of the j th reaction. h_{eff} is the effective heat transfer coefficient with the discharge walls having temperature T_w , and d_{gap} is the electrode separation. The first and second terms in equation (2) account for heating due to momentum transfer collisions with electrons and dissociative electron impact processes which produce Frank-Condon heating. We estimated that $h_{\text{eff}} \approx 23 \text{ W m}^{-2} \text{ K}^{-1}$ based on flow over a flat plate [40].

The external circuit used to drive the DBD is shown in figure 1(b). The storage capacitance is C_s and the peaking capacitor is C_p . The plasma in the DBD is modelled as a resistor R_p and the capacitances of the polymer and the dielectrics on the electrodes are collectively represented by the capacitor C_d . The inductor L is added to obtain the desired LC time constant for the circuit. A ballast resistance R_s may be used to control the energy deposition in the plasma.

The reaction mechanism for plasma-polymer interactions is implemented using a quasi-homogeneous model which distinguishes two regions above the polymer surface; a homogeneous bulk gas phase and a gas-surface boundary layer, as shown in figure 1(c). The radical concentration profile in the boundary layer is mainly driven by diffusion and surface reactions. A gas phase species i is characterized by its density

in the bulk of the gas phase, n_{ig} , and near the surface of the polymer, n_{is} . The state of the polymer is characterized by the fractional occupancy of its surface sites by different species.

The time-evolution of the bulk density of species i is given by

$$\frac{dn_{ig}}{dt} = W_{ig} + W_{id}, \quad (3)$$

where W_{ig} and W_{id} are the net rate of production of species i by the gas phase reactions and diffusion through the boundary layer. Assuming Fick's law for diffusion,

$$W_{id} = \left(-D_i \frac{n_{ig} - n_{is}}{\delta} \right) \left(\frac{S}{V} \right), \quad (4)$$

where D_i is the diffusion coefficient, δ is the boundary layer thickness, S is the polymer geometric surface area and V is the volume of the bulk plasma. The diffusion boundary layer thickness may be taken to be a few mean free paths (microns for air at 1 atm). For the conditions of this study, diffusion is not the rate limiting step and hence the thickness of the diffusion boundary layer is not critical.

Since gas phase chemistry is neglected in the boundary layer, the time variation of the density near the polymer surface is governed by the balance between the fluxes of species entering the boundary layer by diffusion and the consumption or production of species by heterogeneous reactions at the polymer surface. The mass balance in the boundary layer is

$$\frac{d}{dt} \left[\frac{1}{2} (n_{ig} + n_{is}) V_B \right] = D_i \frac{n_{ig} - n_{is}}{\delta} S + (R_{di} - R_{ai}) S, \quad (5)$$

where V_B is the volume of the boundary layer. R_{di} and R_{ai} are the rates of desorption, and adsorption and abstraction per unit surface of polymer for species i . The net rate of consumption by adsorption and abstraction is

$$R_{ai} = \sum_j a_{ij}^{(1)} \gamma_j v_i \frac{n_{is}}{4} - \sum_j a_{ij}^{(2)} \gamma_j v_j' \frac{n'_{js}}{4}, \quad \gamma_j = \gamma_{j0} \frac{\rho_j}{\rho_0}, \quad (6)$$

where γ_j is the adsorption probability for the j th process, and v_i the thermal speed of species i at the surface of the polymer, $v_i = \sqrt{8kT_g/\pi M_i}$. γ_{j0} is the adsorption probability per unit area, ρ_j is the density of surface sites available to reaction j and ρ_0 is the density of surface sites on a virgin polymer surface. $a_{ij}^{(1)}$ and $a_{ij}^{(2)}$ denote the left-hand side (LHS) and right-hand side (RHS) stoichiometric coefficients of species i in reaction j . v_j' and n'_{js} are the thermal speed and density of the gas phase species in the LHS of reaction j . In equation (6), the first sum is for consumption by adsorption and abstraction reactions and the second sum is for production by abstraction reactions. The production rate of species i due to desorption reactions is

$$R_{di} = \sum_j (a_{ij}^{(2)} k_j N_{is}), \quad (7)$$

where k_j is the rate of the j th desorption reaction, and N_{is} is the surface density of the surface species. Although the model can also address adsorption and desorption without reaction, that is physisorption, our reaction mechanism does not include such reactions. In this discussion, desorption refers to species leaving the surface following reactions. The consequences of physisorption are largely site blocking, where the presence of the physically adsorbed species prevents reactions with surface sites by other species.

The densities of the surface species are obtained from

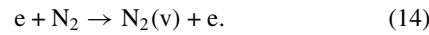
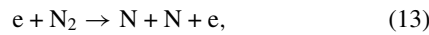
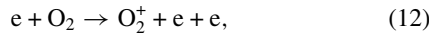
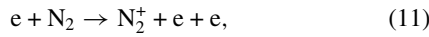
$$\frac{dN_{is}}{dt} = \sum_j \left(a_{ij}^{(2)} \gamma_j v_i \frac{n_{is}}{4} \right) - \sum_j \left(a_{ij}^{(1)} k_j N_{is} \right) + \sum_j \left(\left(a_{ij}^{(2)} - a_{ij}^{(1)} \right) k_j \prod_l N_{ls}^{a_{ij}^{(l)}} \right), \quad (8)$$

where the first sum is over adsorption or abstraction reactions, the second over desorption reactions, and the third over reactions between surface species. n_{is} is the density of the gas phase species involved in the adsorption or abstraction reaction.

The ordinary differential equations for electron temperature (equation (1)), gas temperature (equation (2)), species density (equations (3), (5), and (8)) along with those for circuit parameters are integrated in time using VODE, a stiff equation solver [41].

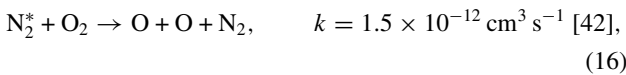
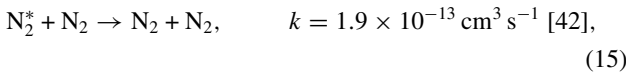
3. Gas phase reaction mechanism for humid-air

Consider humid-air plasma treatment of PP having $N_2/O_2/H_2O = 79/20/1$ (1% H_2O corresponds to a RH of approximately 30% at 300 K, 1 atm). The fractional energy deposition by electron impact processes as a function of electric field/total gas number density (E/N) is shown in figure 2 (at 300 K, 1 atm, $N \approx 2.4 \times 10^{19} \text{ cm}^{-3}$). The current pulse typically lasts a few nanoseconds during which $E/N \approx 300\text{--}600 \text{ Td}$ (1 Td = 1 Townsend = $1.0 \times 10^{-17} \text{ V cm}^2$). For these E/N , energy is dissipated mainly by electronic excitation and ionization of N_2 and O_2 , dissociation of N_2 , and vibrational excitation of N_2 ,



In equations (9) and (10), N_2^* and O_2^* represent the sum of excited states of N_2 and O_2 . We used $N_2(A)$ and $O_2(^1\Delta)$ for their characteristics.

Most of the N_2^* relaxes to N_2 by collisions with N_2 while some collide with O_2 to produce O atoms,



where k is the rate coefficient for the reaction. Most of the O_2^* is consumed by the reaction with O_3 (ozone), while a smaller fraction is quenched by collisions with N_2 ,

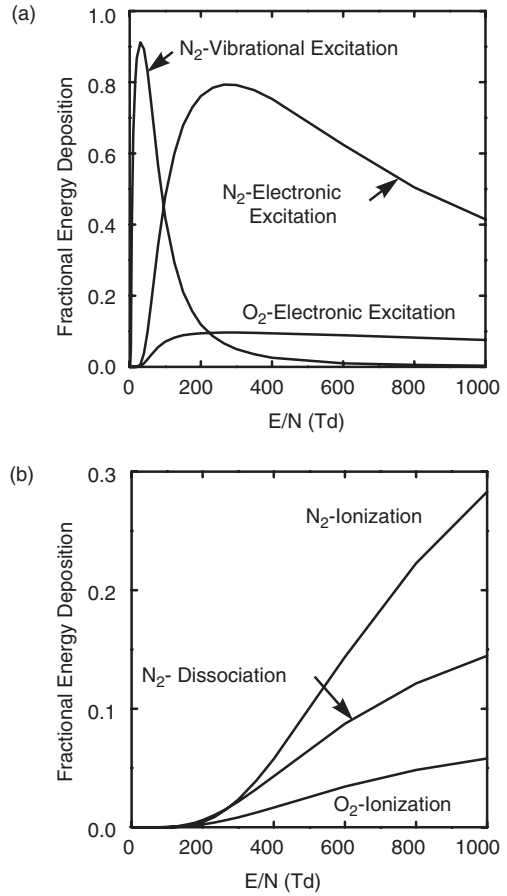
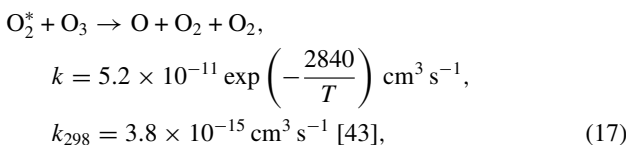
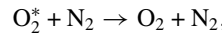


Figure 2. Fractional disposition of energy deposition by electron impact processes as a function of electric field/gas number density (E/N) (1 Td = $1.0 \times 10^{-17} \text{ V cm}^2$). Conditions are: $N_2/O_2/H_2O = 78.9/20.0/1.1$, 1 atm, 300 K. The E/N s of interest are 300–600 Td. (a) Electronic and vibration excitation. (b) Dissociation and ionization.

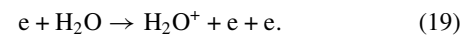


$$k = 3.0 \times 10^{-18} \exp\left(-\frac{200}{T}\right) \text{ cm}^3 \text{ s}^{-1},$$

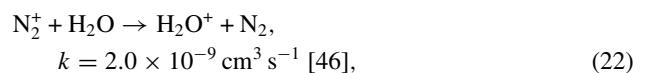
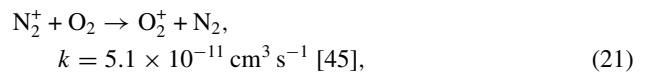
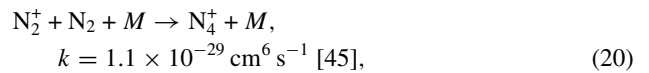
$$k_{298} = 1.5 \times 10^{-18} \text{ cm}^3 \text{ s}^{-1} [44], \quad (18)$$

where k_{298} is the reaction rate coefficient at 298 K.

The reaction mechanism for the charged species is shown in figure 3(a). The initiation reactions are the ionization of N_2 , O_2 , and H_2O producing secondary electrons, N_2^+ (equation (11)), O_2^+ (equation (12)) and H_2O^+ ,



Most of the N_2^+ reacts with N_2 to form N_4^+ while some N_2^+ undergo charge exchange with O_2 and H_2O to produce O_2^+ and H_2O^+ ,



where M represents any other species.

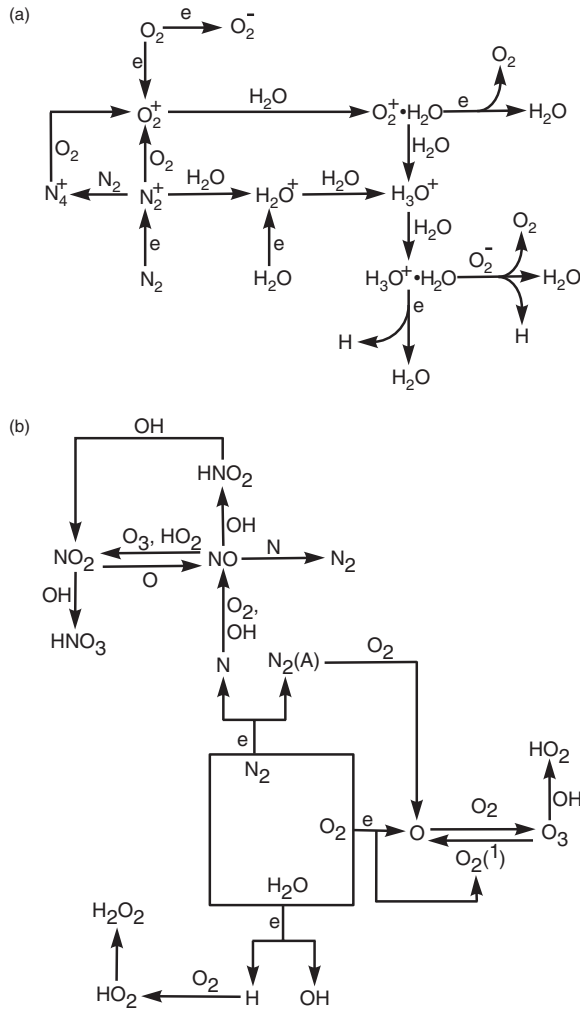
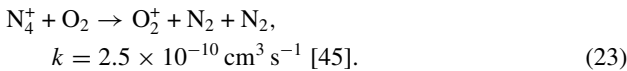
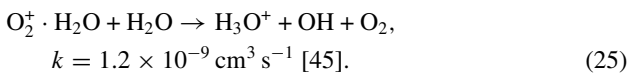
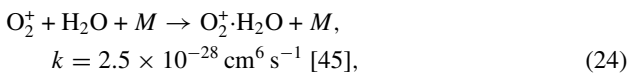


Figure 3. Reaction mechanism for gas phase chemistry in humid-air plasma. (a) Charged species chemistry. (b) Free radical chemistry.

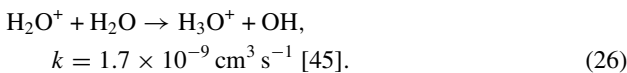
O_2^+ is also formed by the dissociative charge exchange reaction of N_4^+ with O_2 ,



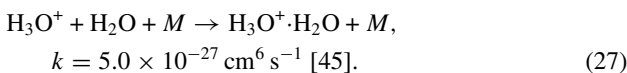
Most of the O_2^+ react with H_2O to form the cluster ion $O_2^+\cdot H_2O$ which further reacts with H_2O to form H_3O^+ ,



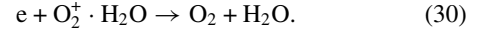
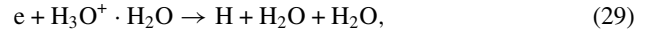
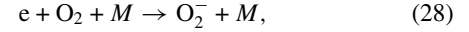
H_2O^+ also reacts with H_2O to form H_3O^+ and OH ,



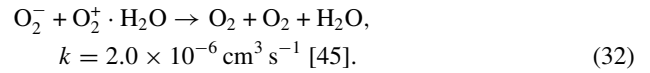
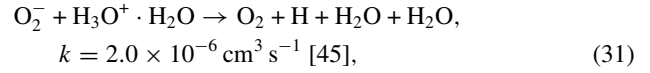
Most of the H_3O^+ then form the cluster ion $H_3O^+\cdot H_2O$ by reaction with H_2O ,



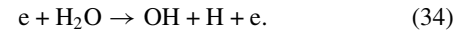
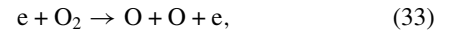
Most of the electrons are lost by three-body attachment to O_2 , while some are consumed by recombination with $H_3O^+\cdot H_2O$ and $O_2^+\cdot H_2O$,



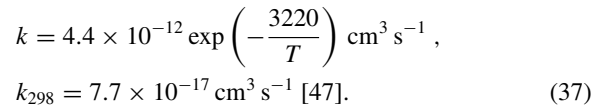
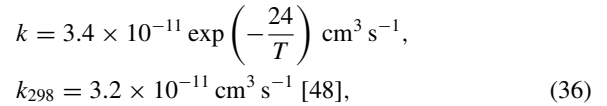
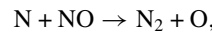
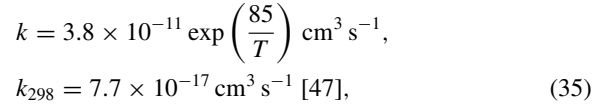
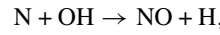
$H_3O^+\cdot H_2O$ and $O_2^+\cdot H_2O$ are also neutralized by reactions with O_2^- forming O_2 , H , and H_2O ,



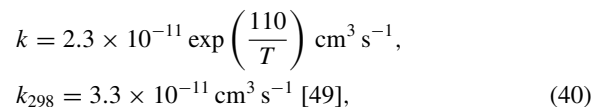
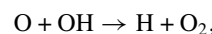
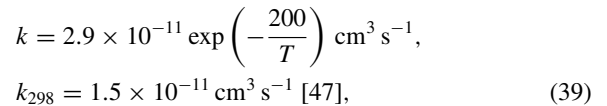
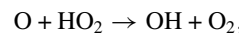
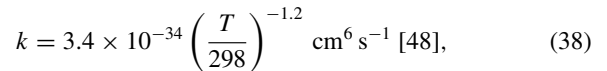
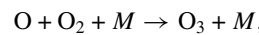
The reaction mechanism developed here for the free radical chemistry in the gas phase is shown in figure 3(b). The initiating reactions are the electron impact dissociations of N_2 (equation (13)), O_2 , and H_2O producing N , O , OH and H ,

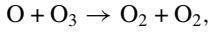


N atoms are consumed by the reactions with OH , NO , and O_2 forming NO and N_2 ,



Apart from the electron impact dissociation of O_2 , other pathways for O production include dissociation of O_2 by N_2^* (equation (16)), and dissociation of O_3 by O_2^* (equation (17)). O atoms are consumed to a large extent by the reactions with O_2 to form O_3 , and to a smaller extent by the reactions with HO_2 , OH , and O_3 ,

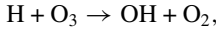




$$k = 8.0 \times 10^{-12} \exp\left(-\frac{2060}{T}\right) \text{ cm}^3 \text{ s}^{-1},$$

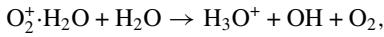
$$k_{298} = 8.0 \times 10^{-15} \text{ cm}^3 \text{ s}^{-1} \text{ [47]}. \quad (41)$$

OH radicals are produced by the electron impact dissociation of H₂O (equation (34)) and by the reactions of H with O₃, O₂⁺·H₂O with H₂O, and O with HO₂,

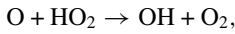


$$k = 1.4 \times 10^{-10} \exp\left(-\frac{470}{T}\right) \text{ cm}^3 \text{ s}^{-1},$$

$$k_{298} = 2.9 \times 10^{-11} \text{ cm}^3 \text{ s}^{-1} \text{ [48]}. \quad (42)$$



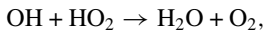
$$k = 1.2 \times 10^{-9} \text{ cm}^3 \text{ s}^{-1} \text{ [45]}. \quad (43)$$



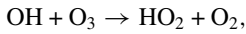
$$k = 2.9 \times 10^{-11} \exp\left(\frac{200}{T}\right) \text{ cm}^3 \text{ s}^{-1},$$

$$k_{298} = 5.7 \times 10^{-11} \text{ cm}^3 \text{ s}^{-1} \text{ [48]}. \quad (44)$$

OH is primarily consumed by the reactions with N (equation (35)) and HO₂ forming NO and H₂O, and secondarily by the reactions with O atoms (equation (40)), O₃, and NO₂,

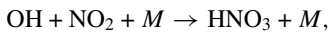


$$k = 8.0 \times 10^{-11} \text{ cm}^3 \text{ s}^{-1} \text{ [48]}. \quad (45)$$



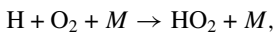
$$k = 1.9 \times 10^{-12} \exp\left(-\frac{1000}{T}\right) \text{ cm}^3 \text{ s}^{-1},$$

$$k_{298} = 6.6 \times 10^{-14} \text{ cm}^3 \text{ s}^{-1} \text{ [50]}. \quad (46)$$



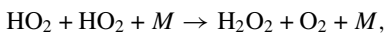
$$k = 2.2 \times 10^{-30} \left(\frac{T}{298}\right)^{-2.9} \text{ cm}^6 \text{ s}^{-1} \text{ [48]}. \quad (47)$$

H atoms are produced by the electron impact dissociation of H₂O (equation (34)) and by the reactions of N with OH (equation (35)), O with OH (equation (40)), and H₃O⁺·H₂O with O₂⁻ (equation (31)). H atoms are mainly consumed by reactions with O₃ to form OH (equation (42)), and by reactions with O₂ to form HO₂,



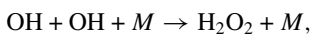
$$k = 1.8 \times 10^{-32} \left(\frac{T}{298}\right)^{-0.8} \text{ cm}^6 \text{ s}^{-1} \text{ [51]}. \quad (48)$$

HO₂ radicals mutually react to produce hydrogen peroxide (H₂O₂), which is also produced by mutual reactions of OH,



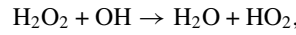
$$k = 1.9 \times 10^{-33} \exp\left(\frac{980}{T}\right) \text{ cm}^6 \text{ s}^{-1},$$

$$k_{298} = 5.1 \times 10^{-32} \text{ cm}^6 \text{ s}^{-1} \text{ [44]}. \quad (49)$$



$$k = 6.9 \times 10^{-31} \left(\frac{T}{298}\right)^{-0.8} \text{ cm}^6 \text{ s}^{-1} \text{ [44]}. \quad (50)$$

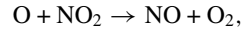
H₂O₂ is consumed by reactions with OH to form H₂O and HO₂,



$$k = 2.9 \times 10^{-12} \exp\left(-\frac{160}{T}\right) \text{ cm}^6 \text{ s}^{-1},$$

$$k_{298} = 1.7 \times 10^{-12} \text{ cm}^3 \text{ s}^{-1} \text{ [44]}. \quad (51)$$

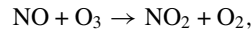
Major N-containing products in the gas phase include NO, NO₂, N₂O, N₂O₅, HNO₂, and HNO₃. NO is produced dominantly by the reactions of N with OH (equation (35)), N with O₂ (equation (37)), and O with NO₂,



$$k = 6.5 \times 10^{-12} \exp\left(\frac{120}{T}\right) \text{ cm}^3 \text{ s}^{-1},$$

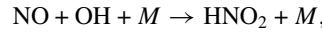
$$k_{298} = 9.7 \times 10^{-12} \text{ cm}^3 \text{ s}^{-1} \text{ [47]}. \quad (52)$$

NO is consumed primarily by reactions with N (equation (36)), O₃, OH, and HO₂, forming N₂, NO₂, HNO₂, and NO₂, respectively,



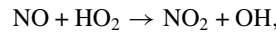
$$k = 4.3 \times 10^{-12} \exp\left(-\frac{1598}{T}\right) \text{ cm}^3 \text{ s}^{-1},$$

$$k_{298} = 2.1 \times 10^{-14} \text{ cm}^3 \text{ s}^{-1} \text{ [52]}. \quad (53)$$



$$k = 8.6 \times 10^{-31} \left(\frac{T}{298}\right)^{-2.5} \exp\left(\frac{34}{T}\right) \text{ cm}^6 \text{ s}^{-1},$$

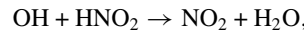
$$k_{298} = 9.7 \times 10^{-31} \text{ cm}^6 \text{ s}^{-1} \text{ [53]}. \quad (54)$$



$$k = 3.5 \times 10^{-12} \exp\left(\frac{240}{T}\right) \text{ cm}^3 \text{ s}^{-1},$$

$$k_{298} = 7.8 \times 10^{-12} \text{ cm}^3 \text{ s}^{-1} \text{ [52]}. \quad (55)$$

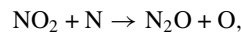
NO₂ is produced mainly by the reactions of NO with O₃ and HO₂ (equations (53) and (55)), and by the reaction of OH with HNO₂,



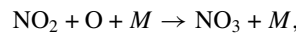
$$k = 1.8 \times 10^{-11} \exp\left(-\frac{390}{T}\right) \text{ cm}^3 \text{ s}^{-1},$$

$$k_{298} = 4.9 \times 10^{-12} \text{ cm}^3 \text{ s}^{-1} \text{ [48]}. \quad (56)$$

Important consumption channels for NO₂ include reactions with OH, O, and N forming HNO₃ (equation (47)), NO (equation (52)), N₂O (nitrous oxide), and NO₃,

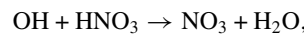


$$k = 2.4 \times 10^{-12} \text{ cm}^3 \text{ s}^{-1} \text{ [45]}. \quad (57)$$



$$k = 9.0 \times 10^{-32} \left(\frac{T}{298}\right)^{-2.0} \text{ cm}^6 \text{ s}^{-1} \text{ [48]}. \quad (58)$$

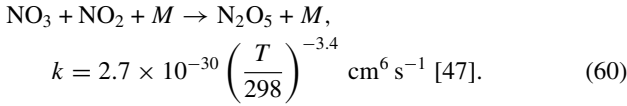
NO₃ is also produced by the reaction of OH with HNO₃,



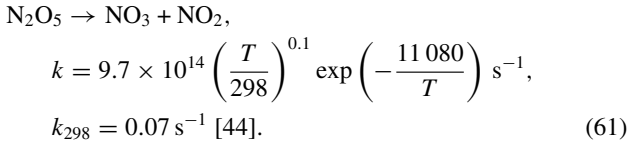
$$k = 1.5 \times 10^{-14} \exp\left(\frac{650}{T}\right) \text{ cm}^3 \text{ s}^{-1},$$

$$k_{298} = 1.3 \times 10^{-13} \text{ cm}^3 \text{ s}^{-1} \text{ [50]}. \quad (59)$$

NO_3 is consumed by the reactions with NO_2 forming N_2O_5 (dinitrogen pentoxide),



N_2O_5 decomposes to regenerate NO_2 and NO_3 ,



HNO_2 is primarily produced by the reaction of OH with NO (equation (54)) and dominantly consumed by the reaction with OH to form NO_2 (equation (56)). HNO_3 is produced by the reaction of OH with NO_2 (equation (47)) and is consumed by the reaction with OH to form NO_3 (equation (59)).

4. Surface reaction mechanism for PP

PP is a saturated hydrocarbon polymer with a carbon backbone containing hydrogen and methyl ($-\text{CH}_3$) groups arranged in an alternating fashion. We used 10^{15} cm^{-2} for the total density of surface sites, as reported for virgin PP [6].

The reactivities of the hydrogen groups in PP depend on the nature of the C atom to which they are attached. There are three types of C atoms in any given monomer unit of PP, primary C, to which only one C atom is bonded; secondary C, to which two C atoms are bonded; and tertiary C, to which three C atoms are bonded (see figure 4(a)). In general, the reactivities of hydrogen bound to these C atoms scale as: $H_{\text{tert}} > H_{\text{sec}} > H_{\text{pri}}$.

A monomer unit of PP consists of two secondary H atoms, a tertiary H atom, and a methyl ($-\text{CH}_3$) group. We acknowledge that these groups are typically configured in such a manner as to minimize the overall surface energy. This

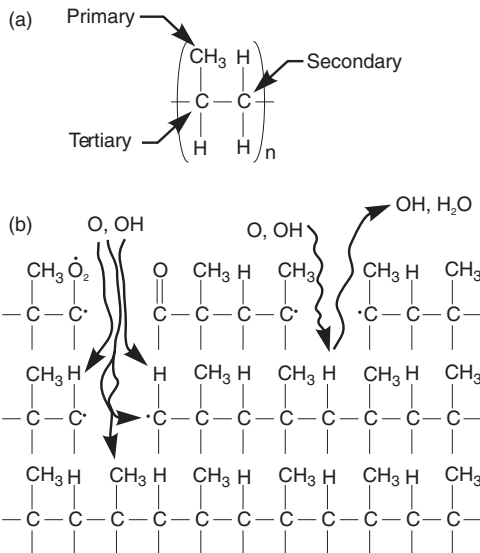


Figure 4. Surface reaction mechanism. (a) A monomer unit in PP. (b) Surface site balance model. PP is a saturated hydrocarbon polymer consisting of two secondary atoms, a tertiary H, and a methyl group attached to a carbon backbone. The total number of surface sites is allowed to vary.

could result in their preferentially being larger proportions of one group on the surface than given by its stoichiometry. However, due to lack of data to differentiate their relative surface concentrations, we assumed a equal likelihood for any of these four groups to be pointing out towards the plasma, and so their initial surface densities are, $N_{\text{H,sec}} = 0.5 \times 10^{15} \text{ cm}^{-2}$, $N_{\text{H,tert}} = 0.25 \times 10^{15} \text{ cm}^{-2}$, and $N_{\text{methyl}} = 0.25 \times 10^{15} \text{ cm}^{-2}$. The total number of surface sites is, however, allowed to vary with treatment time. When a ‘hole’ is made in the PP chain, the diffusing species are allowed to react with the newly formed dangling bonds in the broken chains as well as with the exposed PP chain below, as shown in figure 4(b).

The plasma surface modification of PP is primarily oxidative by reactions with free radicals in the gas phase. The reactions with gas phase ions can be neglected in comparison. The loss frequencies for ions in the gas phase are orders of magnitude larger than their loss frequencies with PP and as a result, ions are preferentially consumed in the gas phase. For example, the loss frequency for $\text{H}_3\text{O}^+ \cdot \text{H}_2\text{O}$ in the gas phase is $\approx 10^7 \text{ s}^{-1}$. For a unit probability for reaction with the PP surface, the loss frequency for $\text{H}_3\text{O}^+ \cdot \text{H}_2\text{O}$ is $\approx 10^4 \text{ s}^{-1}$. The fluxes of free radicals to the surface are at least three orders of magnitude larger than those of ions. For reactions of ions to be comparable to those of free radicals, their reaction probabilities would need to greatly exceed those of free radicals. As reaction probabilities of free radicals are typically $> 10^{-2}$, those for ions would need to be near unity. Having said that, there may be unique reactions which only ions can initiate by virtue of the large activation energy and, in some cases, kinetic energy they bring to the surface; and there is evidence that plasma modification of polymers is sensitive to the ratio of neutral to ionized species [14]. For our conditions, the ions arriving at the PP surface are thermal due to the collisional sheath and so do not contribute to energy activated reactions such as sputtering. On this basis, we have not differentiated ions from the free radicals with respect to their reactivities.

The surface reaction mechanism for PP is given in table 1. In general, the reactions can be classified as: initiation, propagation, and termination.

4.1. Initiation

The initiating reactions are abstractions of hydrogen from the PP chain. Although the cleavage of PP at the C–C bond is possible, the resulting radicals, due to their mutual proximity have been found to quickly recombine to yield back the polymer. Potentially, the species in the gas phase that can react with PP are O_2^* , O_3 , H, N, HO_2 , O, and OH. Investigations have shown that O_2^* reactions on saturated hydrocarbons are slow at best [54]. The rate constant for O_3 reactivity on PP is $1.3 \times 10^{-22} \text{ cm}^3 \text{ s}^{-1}$ [55], which is at least a few orders of magnitude smaller than both the rate constant for the gas phase consumption of O_3 and the rate constant for the reaction of O or OH with PP (which is $\approx 10^{-11} \text{ cm}^3 \text{ s}^{-1}$ [48]). The reactivities for H abstraction by H atoms are two to four orders of magnitude smaller than those for O or OH and hence, H atoms are less likely to be a significant source of H abstraction [56]. Similarly, the reactivities of N and HO_2 towards PP are significantly smaller compared to those of O and OH and so can be safely neglected. Direct oxidation by molecular oxygen

Table 1. Surface reaction mechanism for PP.

Reaction ^a	Probabilities or reaction rate coefficient ^b	Comments
Initiation		
$O_g + PP-H \rightarrow PP^\bullet + OH_g$	$10^{-3}, 10^{-4}, 10^{-5}$	c
$OH_g + PP-H \rightarrow PP^\bullet + H_2O_g$	0.25, 0.05, 0.0025	c
Propagation		
$PP^\bullet + O_g \rightarrow PP-O^\bullet$	$10^{-1}, 10^{-2}, 10^{-2}$	c
$PP^\bullet + O_{2,g} \rightarrow PP-O_2^\bullet$	$1.0 \times 10^{-3}, 2.3 \times 10^{-4}, 5.0 \times 10^{-4}$	c
$PP^\bullet + O_{3,g} \rightarrow PP-O^\bullet + O_{2,g}$	1.0, 0.5, 0.5	c
$PP-O_2^\bullet + PP-H \rightarrow PP-OOH + PP^\bullet$	$5.5 \times 10^{-16} \text{ cm}^2 \text{ s}^{-1}$	
$PP-O^\bullet \rightarrow \text{aldehydes} + PP^\bullet$	10 s^{-1}	
$PP-O^\bullet \rightarrow \text{ketones} + PP^\bullet$	500 s^{-1}	
$O_g + PP=O \rightarrow OH_g + \bullet PP=O$	0.04	
$OH_g + PP=O \rightarrow H_2O_g + \bullet PP=O$	0.4	
$O_g + \bullet PP=O \rightarrow CO_{2,g} + PP-H$	0.4	
$OH_g + \bullet PP=O \rightarrow (OH)PP=O$	0.12	
$PP-O^\bullet + PP-H \rightarrow PP-OH + PP^\bullet$	$8.0 \times 10^{-14} \text{ cm}^2 \text{ s}^{-1}$	
$O_g + PP-OH \rightarrow PP-O + OH_g$	7.5×10^{-4}	
$OH_g + PP-OH \rightarrow PP-O + H_2O_g$	8.2×10^{-3}	
Termination		
$H_g + PP^\bullet \rightarrow PP-H$	0.2, 0.2, 0.2	c
$OH_g + PP^\bullet \rightarrow PP-OH$	0.2, 0.2, 0.2	c

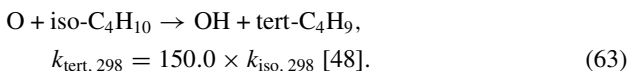
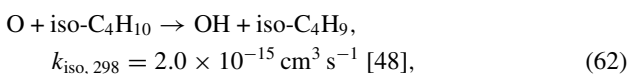
^a Subscript g denotes gas phase species. PP-H denotes PP.

^b Those coefficients without units are reaction probabilities.

^c Reaction probabilities for tertiary, secondary, and primary radicals, respectively.

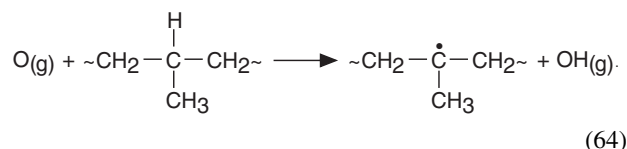
has high activation energies requiring gas temperatures above 700 K to be important. As a result, these processes are not considered here.

OH has been observed spectroscopically during the oxidation of hydrocarbon polymers by atomic oxygen as evidence of H-abstraction [27]. H can be abstracted from any of the primary, secondary, and tertiary sites in PP. The probability of abstraction scales as $H_{\text{tert}} > H_{\text{sec}} > H_{\text{pri}}$ and this ranking is generally independent of the nature of the attacking radical [57]. This trend is supported by the observation that oxidative attack in atactic PP (a configuration of PP in which the methyl groups are placed randomly on both sides of the chain) at tertiary sites is ≈ 20 times faster than at secondary sites [58]. Another example is the abstraction of H from isobutane (iso-C₄H₁₀) by O atoms,



The rate of tertiary H abstraction is 150 times larger than that of secondary H. Similar trends have been observed in reactions of O with n-heptane where rate constants for abstraction of secondary hydrogen are approximately two orders of magnitude larger than those for primary hydrogen [48].

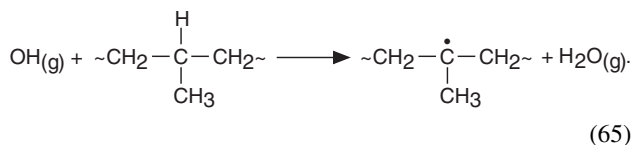
O atoms abstract H from PP to produce a PP alkyl radical and OH,



(The tilde denotes a species in the PP backbone, and (g) denotes gas phase species). Based on the work by Gomez *et al* [59],

at atmospheric pressure, the surface reaction probability for this process is < 0.01 . For this work, we used $\gamma_{\text{tert}} = 10^{-3}$, $\gamma_{\text{sec}} = 10^{-4}$, and $\gamma_{\text{pri}} = 10^{-5}$.

OH radicals also abstract H from PP to produce an alkyl radical and H₂O,

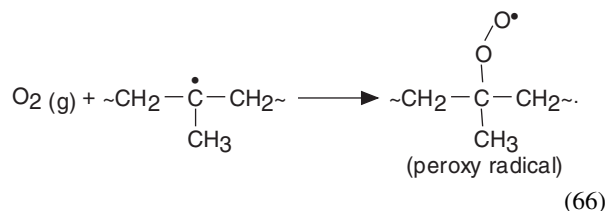


As reaction probabilities for H abstraction by OH are not well known, estimates were obtained based on analogies with rate constants for gas phase reactions of OH with long chain saturated hydrocarbons. The rate constant for the reaction of OH with large hydrocarbon molecules (e.g. C₁₆H₃₄) is $\approx 2.5 \times 10^{-11} \text{ cm}^3 \text{ s}^{-1}$ [48]. A gas-kinetic rate constant is $\approx 10^{-10} \text{ cm}^3 \text{ s}^{-1}$. Assuming that a unit surface reaction probability corresponds to a gas phase kinetic rate constant, the surface reaction probability for H abstraction from PP by OH can be estimated as $\gamma_{\text{tert}} = 0.25$. Also, the branching ratios for H abstractions from the tertiary, secondary, and primary sites of long chain saturated hydrocarbons in the gas phase are such that $k_{\text{tert}}/k_{\text{sec}} \approx 5$ and $k_{\text{sec}}/k_{\text{pri}} \approx 20$ [48]. Therefore, we estimated that $\gamma_{\text{sec}} = 0.05$ and $\gamma_{\text{pri}} = 0.0025$.

This method of deriving surface reaction probabilities typically provides only an estimate. There are other factors such as the orientation of the reactant with respect to the surface, its angle of incidence, and the catalytic activity of the surface which influence the surface reaction probabilities. For a strong interaction with the surface, this approach likely provides a reasonable lower limit to the reactivity because of the neglect of the catalytic effect of the surface. For a weak interaction, this method provides a better estimate. If the reactions are sterically hindered, this method provides an upper limit.

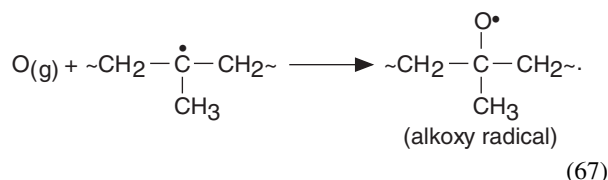
4.2. Propagation

The PP alkyl radicals produced by H abstraction by O and OH (equations (66) and (67)) react with O₂ to form PP peroxy radicals,

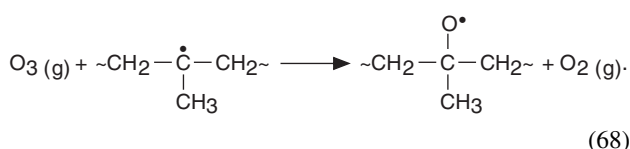


The reactivity of O₂, however, depends on the nature of the alkyl radicals. Studies by Kuzuya *et al* [60] showed that mid-chain alkyl radicals are much less reactive with O₂ compared to end-chain alkyl radicals. The reactions with end-chain radicals are usually diffusion controlled [57] and can be taken to occur at close to the encounter frequency [61].

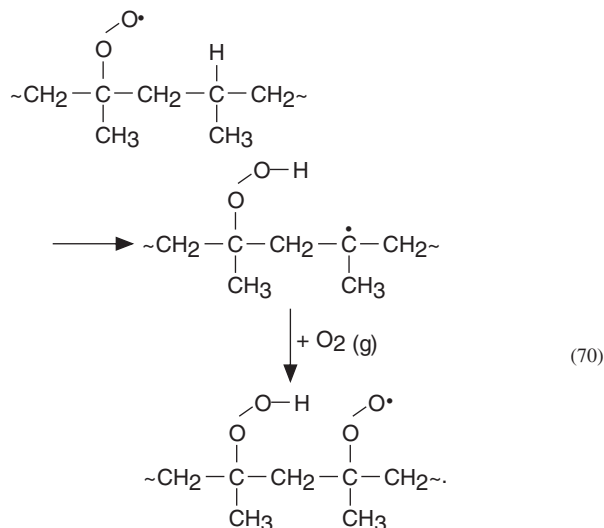
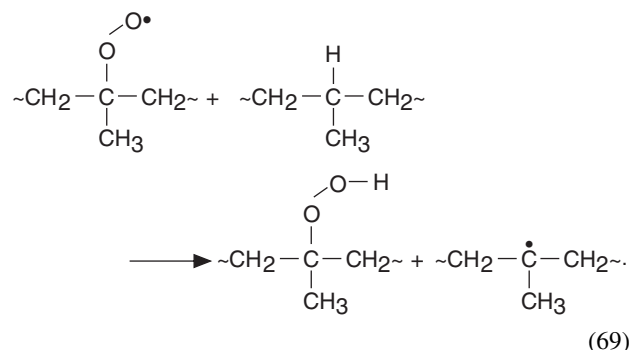
The PP alkyl radicals can also react with O to form alkoxy radicals [27],



This direct pathway to the formation of alkoxy radicals is not significant in corona discharges. Hydrocarbon alkyl radicals are known to react with O₃ in the gas phase at a rate up to five times faster than O₂ [62]. The analogous process for the reactions of O₃ with alkyl surface groups could be a possible route to alkoxy radical formation,



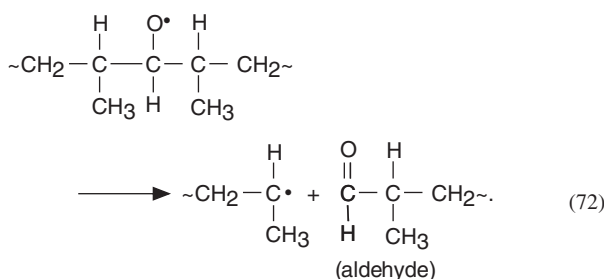
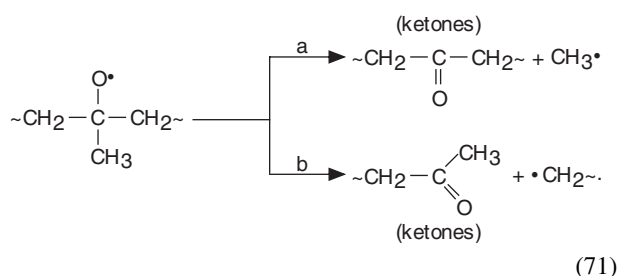
The PP peroxy radicals abstract hydrogen from other polymer chains or from neighbouring sites on the same chain to yield PP hydroperoxides [57]. The ratio of intermolecular to intramolecular attack on the H sites by peroxy radicals is ≈1 : 13 [54]. The intramolecular attack, being more favoured, leads to sequences of neighbouring hydroperoxide groups along a backbone. This series of reactions has been observed during the early stages of oxidation of PP [54],



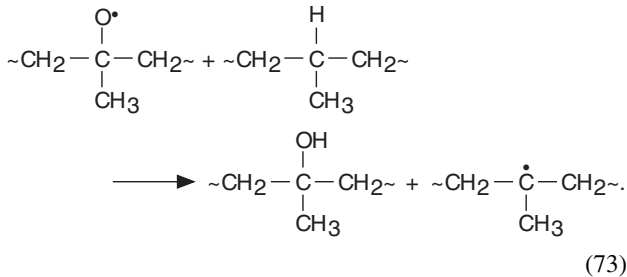
The resulting alkyl radicals then react with abundant O₂ to form peroxy radicals.

The mean time for the reaction of polymer peroxy radicals between propagation steps, based on their reaction with neighbouring tertiary radicals, is ≈5 s [54]. Decomposition of the resulting hydroperoxides leads to a variety of oxidized functional groups [57]. This decomposition, is however slow compared to the formation of alkoxy or peroxy radicals. For example, Poncin-Epaillard *et al* [29] exposed PP previously treated by a N₂ plasma to O₂. Hydroperoxides were formed, with densities up to 10¹⁶ cm⁻², which then decomposed with a half life of 30 h. This long term decomposition of the hydroperoxides is excluded from the reaction mechanism as the residence times for the conditions of interest are at best a few seconds. However, it should be noted made that the hydroperoxides are not necessarily the end products.

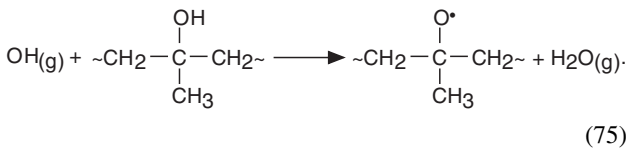
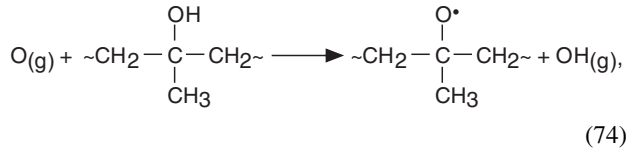
Polymer alkoxy radicals (PO•) are the main source of the chain backbone scission that typically occurs during the oxidation of PP [57, 63]. The rate coefficient for the β-scission of PP alkoxy radicals is ≈10³ s⁻¹ [54]. Such β-scissions on tertiary carbon atoms lead to the formation of ketones while those on secondary carbon atoms result in aldehydes,



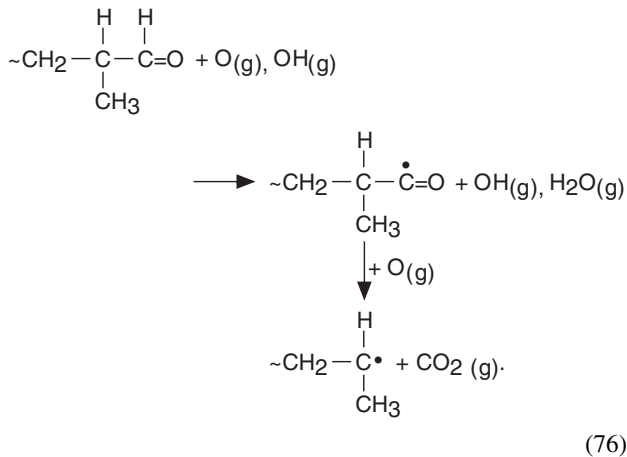
In the β -scission of tertiary alkoxy radicals (equation (71)), channel (b) is more favourable because the resulting secondary polymer hydrocarbon radical is more stable than the primary $\text{CH}_3\bullet$ radical formed by channel (a). β -scission is known to account for only 65% of the alkoxy degradation. The remaining alkoxyes react with the PP matrix to produce alcohol groups [64].



Further reactions of the alcohol groups with O and OH radicals regenerate alkoxy radicals,



Ablation of PP to produce gas phase products is initiated by the abstraction of H in the aldehyde groups by O or OH to produce carbonyl radicals. These carbonyl radicals further react with O atoms to produce CO_2 and PP alkyl radicals,



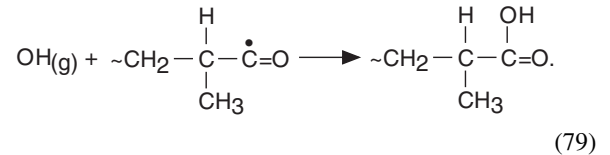
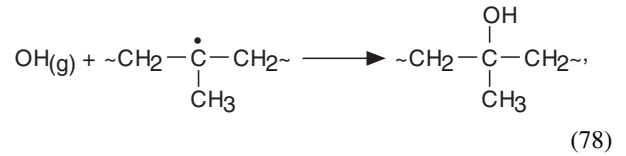
The etched product CO_2 exposes the site beneath for further oxidation.

4.3. Termination

While hydrogen atoms are less likely than O or OH to abstract H from PP, they compete with O and OH for the PP alkyl radicals [10],



Reactions of OH with alkyl and carbonyl radicals result in the formation of alcohols and acids,



These reactions are considered terminal because of the higher stability of the end products compared to the free radicals.

We acknowledge that there are additional surface reaction processes such as cross-linking, reactions initiated by UV radiation from the plasma [57], and reactions resulting in unsaturation in the carbon backbone. Although these reactions can mechanically be incorporated into the model, we chose not to include them in part due to lack of fundamental data and in part by our conclusions that for our operating conditions the dominant reaction pathways are those discussed here. For example, in other work, the contributions of UV radiation to surface modification for these conditions were estimated to be small [65]. In this regard, operating with significantly different conditions open up new reaction pathways. For example, low-pressure capacitively coupled radio frequency discharges have significantly higher ratios of ion-to-radical fluxes, the ions have super-thermal energies and UV radiation is plentiful, and so a different hierarchy of reactions may be important [66].

5. Plasma surface modification of PP

To validate the surface reaction mechanism, comparisons were made to experiments conducted by O'Hare *et al* [25] for humid-air plasma treatment of PP. The gas composition was $\text{N}_2/\text{O}_2/\text{H}_2\text{O} = 78.9/20.0/1.1$, at 1 atm and initially 300 K (1.1% H_2O corresponds to a RH of $\approx 30\%$). The downstream electrode length is 12 cm and the PP web speed is 250 cm s^{-1} producing a gas residence time of 0.05 s. The applied voltage is sinusoidal at 9.6 kHz across a 3 mm gap providing 460 voltage pulses per site. The energy deposition was varied ($0-1.5 \text{ J cm}^{-2}$) by changing the applied voltage ($0-20 \text{ kV}$). The base case uses 0.8 J cm^{-2} .

The electron density (n_e) and electron temperature (T_e) for the first, last, and select intermediate pulses as a function of time for the base case are shown in figure 5. The timescale is relative to the beginning of each voltage pulse. During the first voltage pulse, the potential across the gap is mainly a result of the applied voltage. The seed electrons accelerated by the electric field gain energy and ionize the background gases, N_2 , O_2 , and H_2O , producing secondary electrons, N_2^+ , O_2^+ , and H_2O^+ (equations (11), (12), and (19)). For the first pulse, the peak electron temperature is 3.4 eV and the peak electron density is $7 \times 10^{12} \text{ cm}^{-3}$.

With the flow of current through the discharge, the dielectric on the surface of the electrodes is charged, thereby removing voltage from the gap and terminating the discharge.

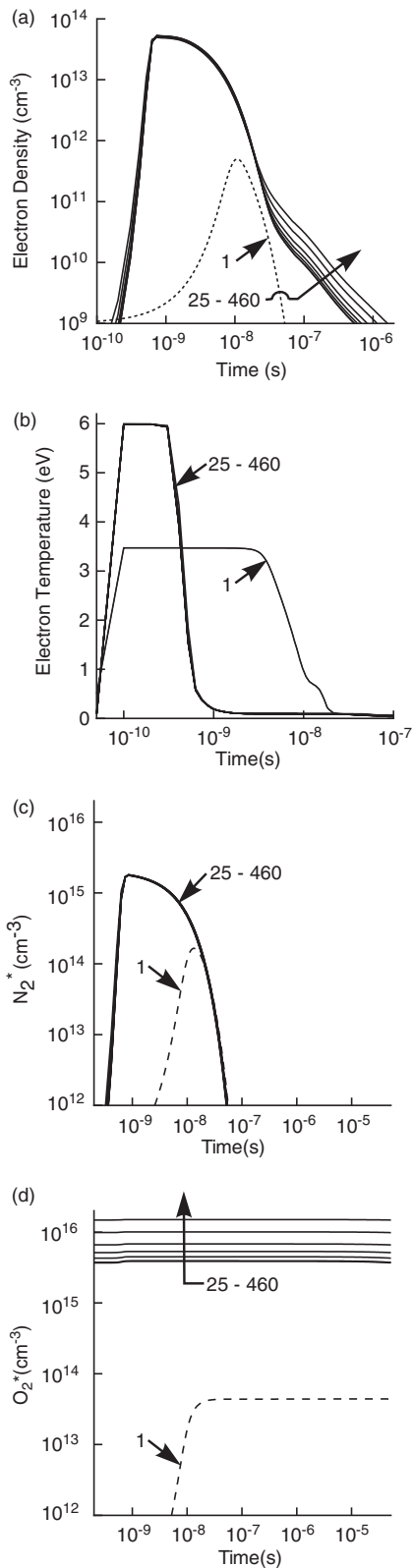


Figure 5. Plasma parameters and densities of excited species for the base case conditions. (a) Electron density (n_e). (b) Electron temperature (T_e). (c) N_2^* . (d) O_2^* . Conditions are $N_2/O_2/H_2O = 78.9/20.0/1.1$, 1 atm, 300 K (1.1% H_2O corresponds to a RH of $\approx 30\%$). The energy deposition is 0.8 J cm^{-2} and the applied voltage is 15 kV. Due to the charging of the dielectric, the T_e and n_e are larger for later pulses. O_2^* being a relatively stable species, has a longer lifetime and its density accumulates with time.

During subsequent pulses, the voltage across the dielectric adds to the gap voltage, enabling a more rapid avalanche and shorter current pulses producing larger n_e ($5 \times 10^{13} \text{ cm}^{-3}$) and T_e (6.0 eV) compared to the first pulse. The differences in n_e after 10^{-7} s for pulses later than the first are due to changes in the composition of the background gases.

The peak E/N during later discharge pulses is $\approx 400 \text{ Td}$ for which nearly 70% of the energy deposition is expended in the electronic excitation of N_2 (equation (9)) and about 10% is expended in the electron excitation of O_2 (equation (10)). The densities of N_2^* and O_2^* during the first, last, and select intermediate pulses as a function of time are shown in figure 5. Most of the N_2^* ($>90\%$) and smaller amounts of O_2^* ($<10\%$) are quenched by collisions with the background gases (equations (15) and (18)). Other channels for N_2^* consumption ($<10\%$) include reactions with O_2 to produce O (equation (16)). The dominant channel for O_2^* consumption is the reaction with O_3 to produce O (equation (17)). O_2^* is less reactive compared to N_2^* and hence, its density accumulates over the pulses.

Other channels for electron energy loss include ionization of N_2 and O_2 to produce N_2^+ and O_2^+ (equations (12) and (13)), whose densities are shown in figure 6. Due to the nearly constant density of N_2 and O_2 and similarity in loss channels, the differences in the densities of N_2^+ and O_2^+ with pulses after the first are small. N_2^+ is lost by association with N_2 to form N_4^+ (equation (20)). N_4^+ charge exchanges with O_2 to form $O_2^+\cdot H_2O$ (equation (23)), which further reacts with H_2O to form $H_3O^+\cdot H_2O$ (equations (25) and (27)). The time dependence of the densities of $H_3O^+\cdot H_2O$ and the dominant negative ion, O_2^- , for the first, last, and select intermediate pulses are also shown in figure 6. O_2^- is produced by the attachment of electrons to O_2 (equation (28)). $H_3O^+\cdot H_2O$ and O_2^- neutralize to yield O_2 , H, and H_2O (equations (31) and (32)).

Electron impact dissociation of the background gases produces N, O, and OH (equations (13), (33), and (34)), whose densities are shown in figure 7. N atoms are consumed by reactions with OH and O_2 (equations (35) and (37)) to produce NO; and with NO to produce N_2 (equation (36)). The contributions of the reactions with OH, NO, and O_2 towards N consumption are 40%, 45%, and 10%, respectively. N being less reactive than other radicals, accumulates in the discharge between to pulses.

The electron impact dissociation of O_2 (equation (33)) accounts for $\approx 25\%$ of the O atom production; while dissociation of O_2 by N_2^* (equation (16)) and O_3 by O_2^* (equation (17)) each contribute $\approx 30\%$. O atoms are primarily consumed by reactions with O_2 ($\approx 85\%$) to form O_3 (equation (38)); and with HO_2 (6%), OH (4%), and O_3 (2%) to produce O_2 (equations (39)–(41)). After a few hundreds of pulses, the density of O reaches a periodic steady state.

Although the initial inventory of OH in a given pulse is created by electron impact dissociation of H_2O (equation (34)), the contribution of this process to the overall production of OH is only 2%. Dominant channels for OH production include reactions of H with O_3 (equation (42)), $O_2^+\cdot H_2O$ with H_2O (equation (43)), and O with HO_2 (equation (44)) with their contributions being 35%, 35%, and 20%, respectively. OH is

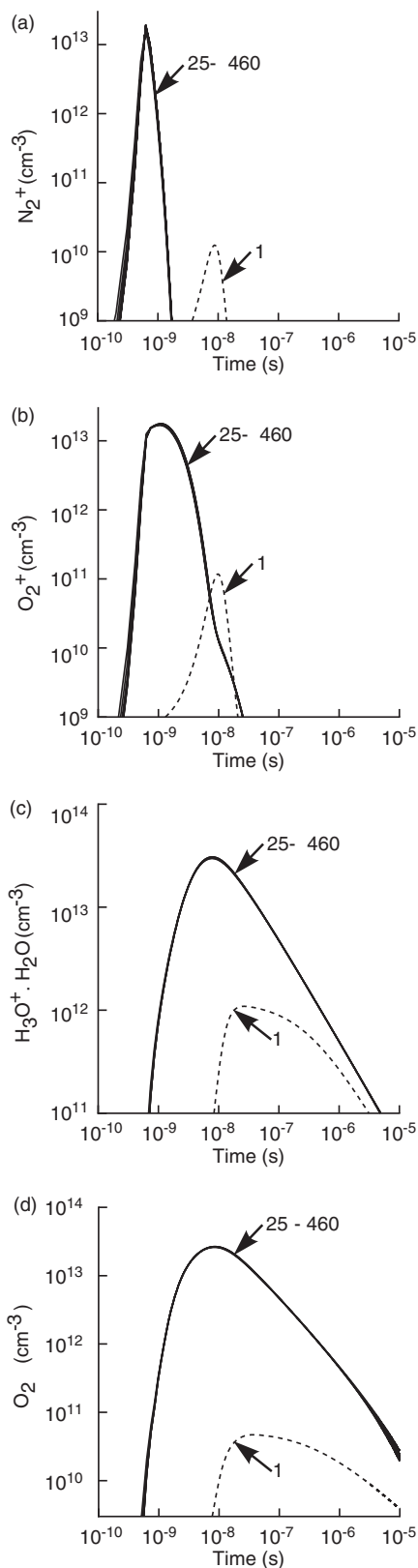


Figure 6. Time dependence of densities of charged species. (a) N_2^+ . (b) O_2^+ . (c) $H_3O^+ \cdot H_2O$. (d) O_2^- . N_2^+ and O_2^+ are formed mainly by the electron impact ionization of N_2 and O_2 . N_2^+ is mainly consumed by reactions with N_2 to form N_4^+ (equation (22)). O_2^+ is primarily consumed by the reactions with H_2O to form the cluster ion $O_2^+ \cdot H_2O$. The end result of the ion chemistry is the production of the $H_3O^+ \cdot H_2O$ and O_2^- .

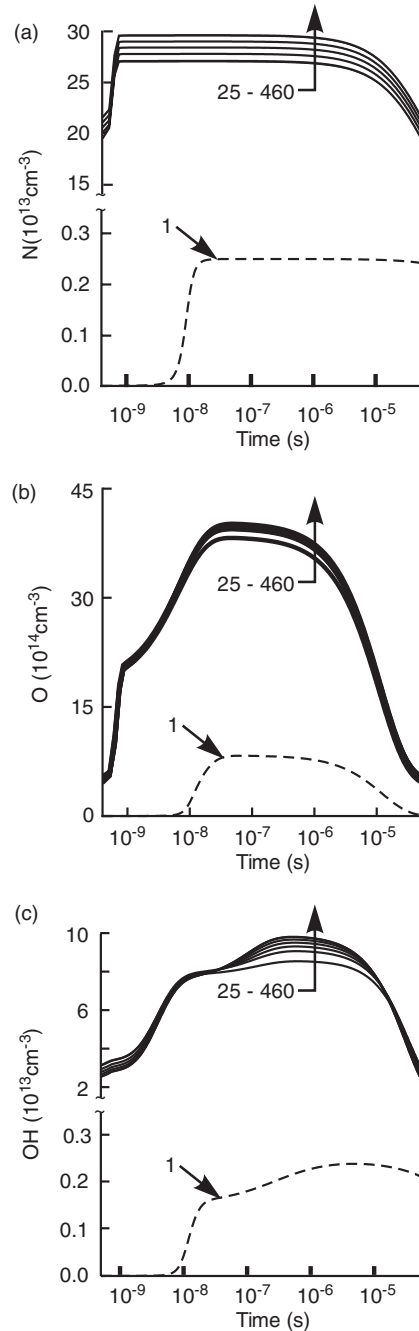


Figure 7. Densities of primary radicals as a function of time. (a) N. (b) O. (c) OH. N being less reactive than O and OH accumulates between pulses. O and OH are largely consumed in the interpulse period.

primarily consumed by the reactions with N (equation (35)) and HO_2 (equation (45)) forming NO ($\approx 30\%$) and H_2O ($\approx 30\%$), respectively; and by the reactions with O (equation (40)), O_3 (equation (46)), and NO_2 (equation (47)) with their contributions being 11%, 18%, and 7%. The density of OH increases with pulses due to the increase in the density of O_3 (see below), which reacts with H to produce OH (equation (42)). Similar to O, the density of OH reaches a periodic steady state after a few hundreds of pulses.

The densities of H, HO_2 , and O_3 as a function of time are shown in figure 8. H atoms are mainly produced by

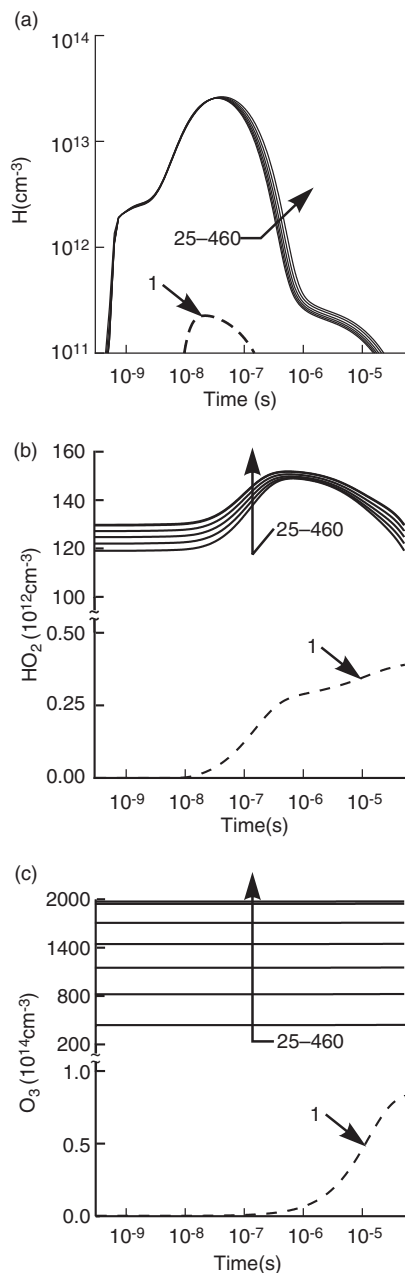


Figure 8. Densities of radicals as a function of time. (a) H. (b) HO₂. (c) O₃. HO₂ and O₃ being less reactive compared to H accumulate over pulses.

the reactions of N with OH (equation (35)), O with OH (equation (40)), and H₃O⁺·H₂O with O₂⁻ (equation (31)), with their contributions being 38%, 15%, and 42%. H atoms primarily react with O₃ to form OH (equation (42)), and with O₂ to form HO₂ (equation (48)). The density of H reaches a periodic steady state within 10 s of pulses.

HO₂ (hydroperoxy) radicals are formed by the reactions of H with O₂ (equation (48)). The production of HO₂ dominantly occurs during the first microsecond. Later, consumption of HO₂ by reactions with HO₂ (equation (49)) and NO (equation (55)) to produce H₂O₂ and NO₂ dominate. As HO₂ is less reactive, its density also accumulates from pulse to pulse.

O₃ is produced by the reaction of O with O₂ (equation (38)) and is primarily consumed by reactions with O₂^{*} (66%,

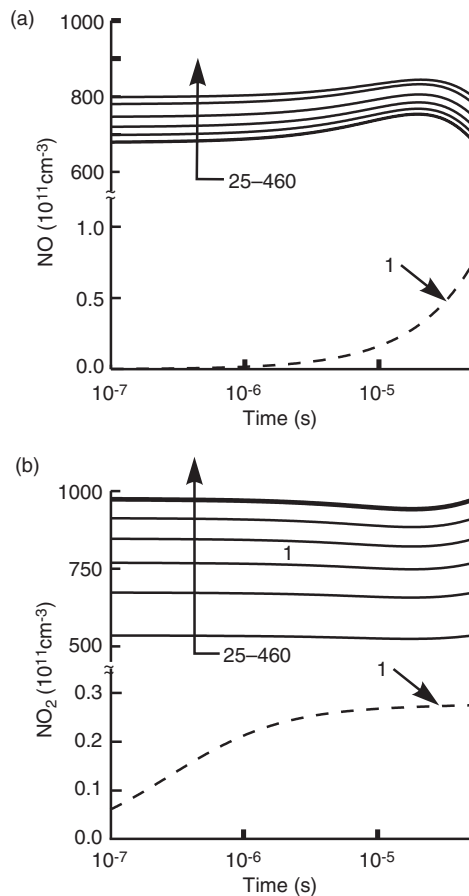


Figure 9. Densities of NO_y as a function of time. (a) NO. (b) NO₂. Most of the NO and NO₂ are converted to HNO₃ (equation (47)) and N₂O (equation (57)).

equation (17)), H (12%, equation (42)), and OH (10%, equation (46)) to form O, OH, and HO₂. The rapid production of O₃ from O and O₂ dominates over losses and so O₃ accumulates from pulse to pulse.

N-containing products in the gas phase include NO and NO₂, whose densities are shown in figure 9. NO is produced by the reactions of N with OH (equation (35)), N with O₂ (equation (37)), and O with NO₂ (equation (31)), with their contributions being 70%, 15%, and 10%. NO is consumed primarily by the reactions with N, O₃, OH, and HO₂ to produce N₂ (equation (36)), NO₂ (equation (53)), HNO₂ (equation (54)), and NO₂ (equation (55)), respectively, with contributions of 60%, 20%, 10%, and 10%. Due to the increase in the density of N and OH with time (see figure 7), more NO is progressively generated by the reaction of N with OH (equation (35)).

NO₂ is produced mainly by the reactions of NO with O₃ and HO₂ (equations (53) and (55)), and OH with HNO₂ (equation (56)), with their contributions being 50%, 22%, and 21%, respectively. NO₂ is primarily consumed by the reactions with OH, O, N forming HNO₃ (equation (47)), NO (equation (52)), and N₂O (equation (57)) with their contributions being 50%, 10%, and 21%. Approximately, 5% of NO₂ is consumed by the reactions with O forming NO₃ (equation (58)). Since the densities of O₃ and N increase with time, the density of NO₂ accumulates over the pulses.

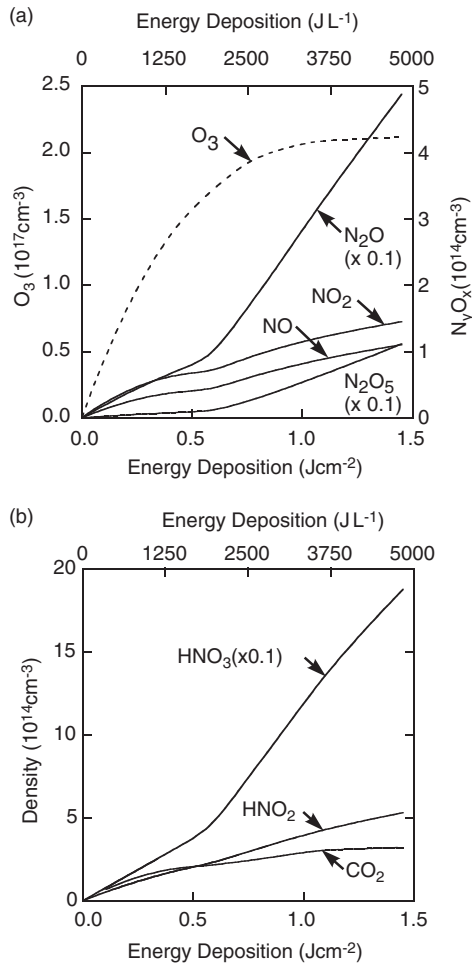


Figure 10. Effect of energy deposition on the exit densities of gas phase species. (a) O_3 and N_yO_x . (b) CO_2 and HNO_x . With increasing energy deposition, larger densities of O, OH, and N are produced thereby increasing the production of O_3 , NO, NO_2 , N_2O_5 , N_2O , HNO_2 , and HNO_3 . The density of CO_2 increases due to increased ablation of PP by O and OH. The energy deposition is varied by changing the applied voltage.

The consequences of varying energy deposition on the exit densities of O_3 , N_yO_x , HNO_x , and CO_2 are shown in figure 10. With increasing energy deposition, larger densities of O, N, and OH are produced. As O_3 is primarily formed by the reaction of O with O_2 (equation (38)), its density increases with increasing energy deposition. Similarly, NO is dominantly produced by the reaction of N with OH (equation (35)) and so the NO production increases. O_3 and NO react to produce NO_2 (equation (53)) and so the density of NO_2 also increases with energy deposition. This further leads to the increased production of N_2O_5 (equation (60)) and N_2O (equation (57)). OH reacts with NO to produce HNO_2 (equation (54)) and with NO_2 to form HNO_3 (equation (47)), and so their densities increase. The density of CO_2 increases due to increased ablation of PP initiated by O and OH (equation (76)).

The relative surface concentrations of alcohol, acid, peroxy, and carbonyl groups on PP as a function of energy deposition are shown in figure 11. With increasing energy deposition, the surface concentrations of the peroxy and acid groups increase and saturate with a small surface coverage,

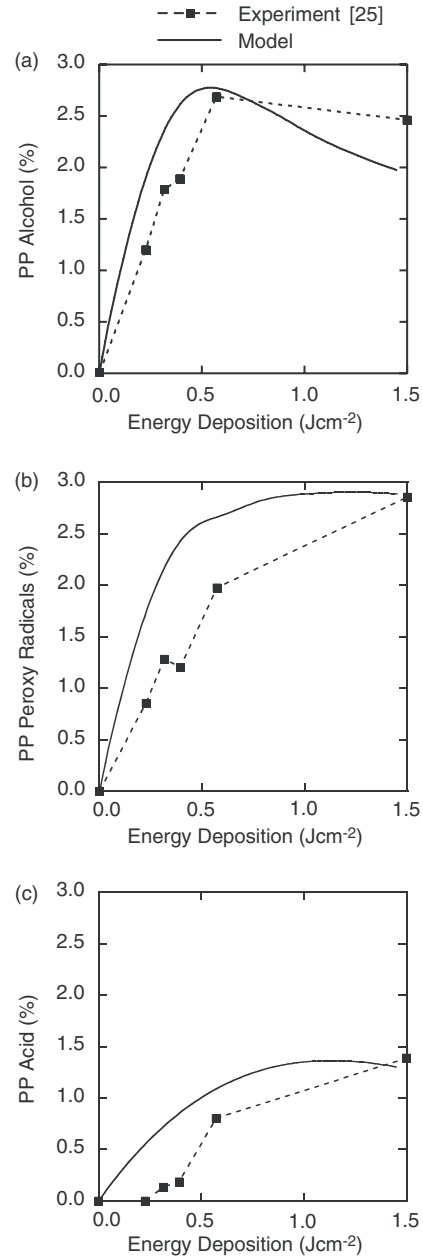


Figure 11. Experimental [25] and modelling results for percentage coverage of PP by functional groups after humid-air corona treatment. (a) Alcohol ($-C-OH$) and acid ($-HO-C=O$). (b) Peroxy ($-C-OO$) and carbonyl ($-C=O$). With increasing energy deposition, the relative surface concentrations of the acid and peroxy groups increase and saturate, while those of the alcohol and carbonyl groups initially increase and then decrease. Conditions are same as in figure 5.

while those of the alcohol groups initially increase and then decrease. The initial increase in the densities of peroxy and acid groups is due to the increased availability of radicals. The saturation of these densities at higher energy deposition is due to the balance between the consumption and production of alkyl radicals, their precursor. The densities of alcohols and carbonyls decrease at higher energy deposition because of consumption by O and OH to form alkoxy radicals and CO_2 (equations (74)–(76)). The computed surface densities of alcohol groups agree well with the experiments of

O'Hare *et al* [25]. The less good agreement for the densities of peroxy and carbonyl groups at high energy deposition is due to the overestimation of the ablation of PP by the model. With larger ablation, more alkyl radicals and subsequently more peroxy radicals are generated. The agreement for the densities of acid groups is within 25%. Although significant amounts of N are produced in the gas phase (see figure 7(a)), N atom incorporation has not been experimentally observed on air plasma treated PP. It is likely that either N is either unreactive towards PP treated in this manner or other processes inhibit the incorporation of N.

The surface densities of the alkyl, peroxy, and alkoxy radicals on PP as a function of time are shown in figure 12. Alkyl radicals are formed by the abstraction of H from PP by O and OH (equations (64) and (65)). Due to the production of O and OH in the gas phase with every discharge pulse

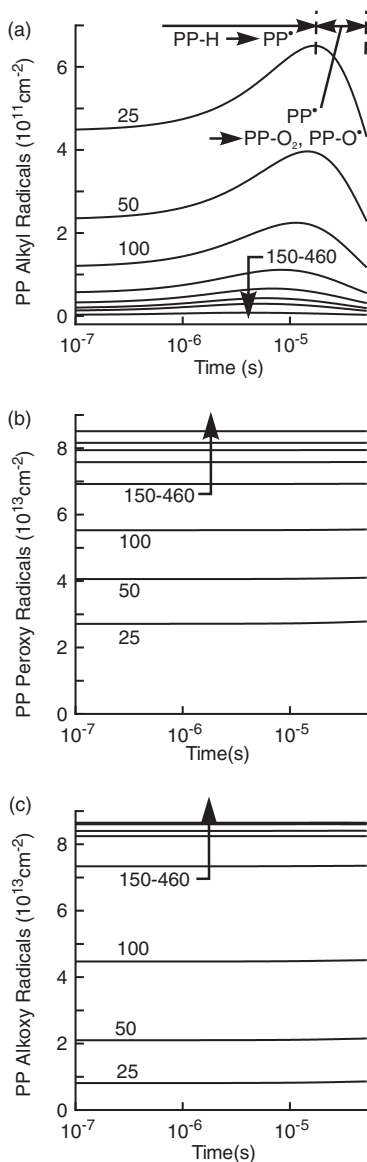


Figure 12. Time dependence of surface densities. (a) Alkyl radicals. (b) Peroxy radicals. (c) Alkoxy radicals. Alkyl radicals are produced by the reaction of O with PP-H (equations (65) and (66)) and are consumed by the reactions with O_2 and O_3 to form peroxy and alkoxy radicals (equations (67) and (69)).

(see figure 7), there is a renewed flux of O and OH to the PP surface and so the alkyl radicals are produced with each pulse. During a given pulse, the production of alkyl radicals dominantly occurs for $t < 20 \mu s$. At later times, these radicals are consumed by the reactions with O_2 and O_3 to form peroxy and alkoxy radicals (equations (66) and (68)). As the free sites on the PP surface are depleted at later pulses, the densities of the alkyl radicals decrease. There is little intra-pulse structure in the densities of alkoxy and peroxy radicals as their densities receive a small increment each pulse.

The surface densities of the alcohol and carbonyl groups on PP as a function of time are shown in figure 13. As with the alkoxy and peroxy radicals, the densities of these species have little intra-pulse structure. The alkoxy radicals react with the hydrogen in the neighbouring sites to produce alcohols (equation (73)). Alcohol groups are consumed by reactions with O and OH in the gas phase to regenerate alkoxy radicals (equations (74) and (75)). Carbonyl groups, namely aldehydes and ketones, are produced by the β -scission of alkoxy radicals (equations (71) and (72)).

Studies by Foulon-Belkacemi *et al* [67] and Strobel *et al* [65] have shown that the surface composition of polymers subjected to humid-air coronas is sensitive to the RH. The time-averaged densities of O and OH (denoted as $\langle O \rangle$ and $\langle OH \rangle$) and the exit density of O_3 are shown in figure 14(a) as a function of RH. For a given energy deposition, with increasing RH, more energy is channelled into H_2O decomposition and so

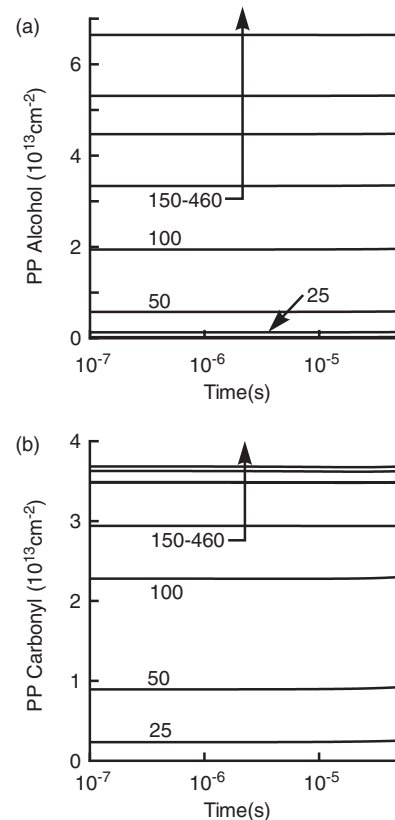


Figure 13. Surface densities as a function of time. (a) Alcohols. (b) Carbonyls. There is little intra-pulse structure. Alcohol groups are produced by the abstraction of H from neighbouring sites on PP by alkoxy radicals (equation (74)). Carbonyl groups are produced by the β -scission of alkoxy radicals (equations (72) and (73)).

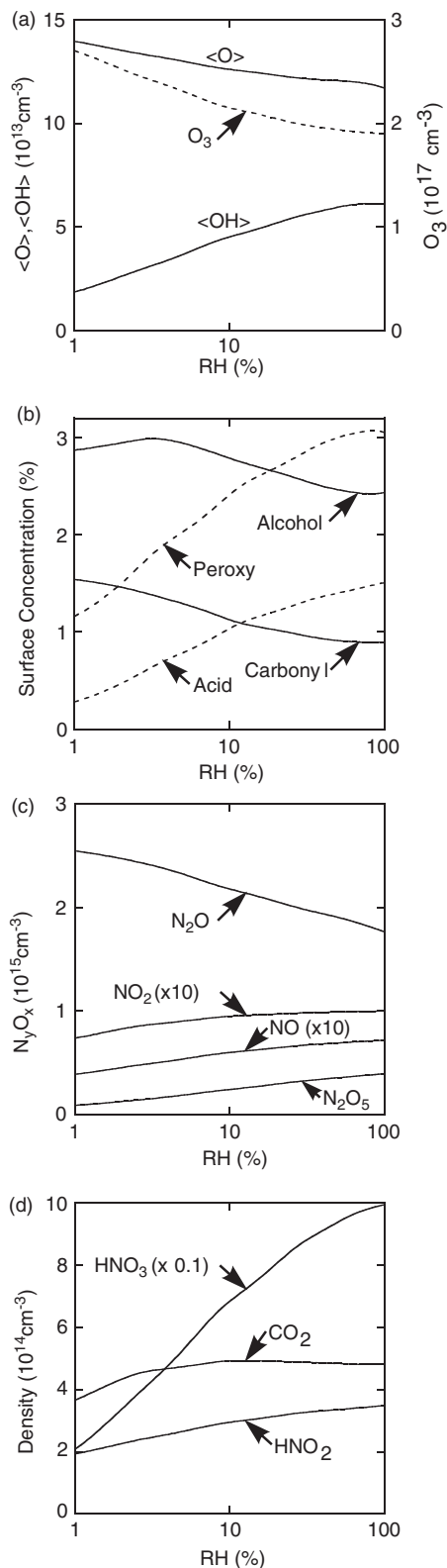


Figure 14. Consequences of varying RH on the exit surface composition of PP and on the time-averaged and exit densities of gas phase species. (a) Time-averaged densities of O and OH (denoted as $\langle O \rangle$ and $\langle OH \rangle$) and exit density of O_3 . (b) Surface concentrations of alcohol, peroxy, carbonyl, and acid groups. (c) Exit $N_j O_x$. (d) Exit CO_2 and HNO_x . Conditions are otherwise the same as in figure 5.

more OH is produced. Correspondingly, the production of O is decreased. This decrease results in decreased O_3 densities, $\approx 30\%$ from RH of 1% to 100%, a trend commonly observed in ozonizers [68]. The relative concentrations of peroxy, alcohol, carbonyl, and acid groups as a function of RH are shown in figure 14(b). Since more OH is produced at larger RH and since OH is more reactive than O, the rate of the initial step of H abstraction from PP is increased and so more alkyl radicals are generated (equation (65)). Since the density of O_3 decreases, PP alkyl radicals are preferentially consumed by O_2 and so larger densities of peroxy radicals are formed. The surface density of the alcohol groups initially increases and then decreases. The increased formation of alkyl radicals and subsequently alkoxy radicals (equations (65) and (68)) result in an initial increase in the surface concentration of alcohols with RH (equation (73)). Due to the decreased flux of O_3 to the PP surface, fewer alkoxy radicals are generated and so production of alcohols and carbonyl radicals decreases (equations (68), (71)–(73)). The densities of alcohols also decrease with RH due to their increased consumption by OH (equation (75)). Similarly, the decrease in carbonyl radicals with RH is in part due to the increased consumption by reaction with OH to form acids (equation (79)).

The densities of NO, NO_2 , $N_2 O_5$, $N_2 O$, HNO_2 , and HNO_3 in the gas phase as a function of RH are shown in figures 14(c) and (d). The densities of NO and NO_2 only slightly increase with RH. Due to the high reactivities of NO and NO_2 , they are mostly converted into species such as HNO_3 (equation (47)), $N_2 O$ (equation (57)), HNO_2 (equation (54)), and $N_2 O_5$ (equation (60)). As NO is dominantly produced by the reaction of N with OH (equation (35)), the increased production of OH with RH increases the density of NO. The density of NO_2 also increases since it is primarily produced from NO (equations (53) and (55)). As a result, the densities of HNO_2 and HNO_3 also increase (equations (47) and (54)). OH further reacts with HNO_3 to produce NO_3 and $H_2 O$ (equation (59)). The increasing densities of NO_3 and NO_2 then produce $N_2 O_5$ (equation (60)). $N_2 O$ is dominantly produced by the reaction of N with NO_2 (equation (57)). NO_2 is preferentially consumed by reaction with OH to form HNO_3 (equation (47)). Therefore, less NO_2 is available for reaction with N and so the production of $N_2 O$ decreases. CO_2 is produced as a result of the ablation of PP (equation (76)). The initial increase in the density of CO_2 with RH is due to the increased production of carbonyl radicals (equation (76)). However, as the density of OH increases with RH, carbonyl radicals are preferentially consumed by reaction with OH to form acids and so the density of CO_2 saturates.

The surface concentrations of alcohols, acids, carbonyl, and peroxy radicals and the densities of the dominant gas phase products as a function of inlet gas temperature are shown in figure 15. The rate constant for the production of O_3 from O decreases with temperature (equation (38)), while the rate constants for the consumption of O_3 (e.g. with NO (equation (53))) increase, resulting in a net decrease of O_3 . This decrease in O_3 results in the decreased formation of alkoxy radicals on the PP surface (equation (68)) and therefore a decreased production of alcohols, carbonyl, and acid groups (equations (71)–(73) and (79)). The small decrease in the density of carbonyl groups does not significantly affect

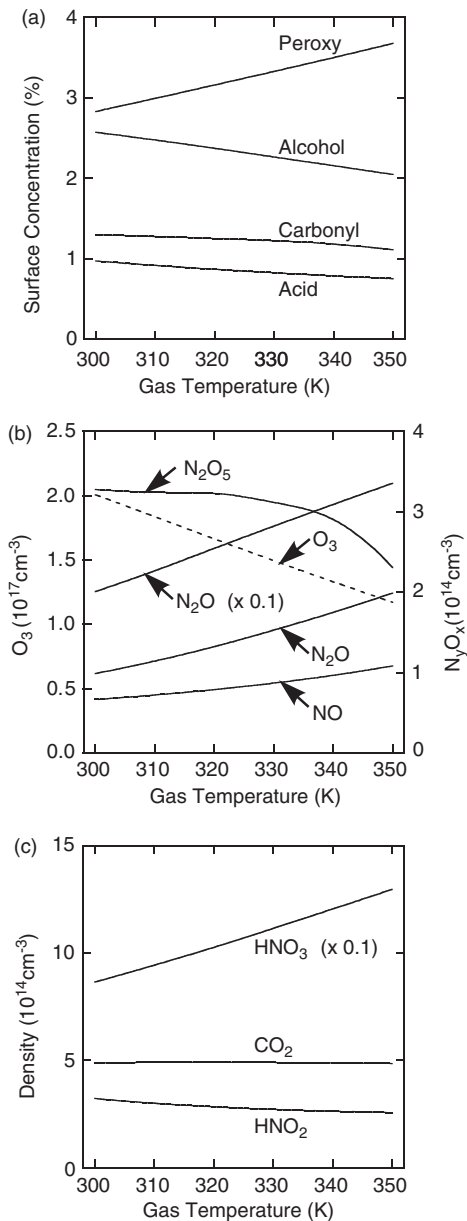


Figure 15. Effects of gas temperature on the exit surface properties of PP and the densities of gas phase products. (a) Surface concentrations of alcohol, peroxy, carbonyl, and acid groups. (b) Exit O_3 and $N_y O_x$. (c) Exit CO_2 and HNO_x . Conditions are otherwise the same as in figure 5.

the ablation process (equation (76)) and so the density of CO_2 remains almost constant. Due to the lower rate of consumption of alkyl radicals by reaction with O_3 with increasing gas temperature, more alkyl radicals are available for reaction with O_2 and so the peroxy radical concentration increases (equation (66)).

The increased rate of reaction of O_3 with NO produces larger densities of NO_2 (equation (53)) and so the density of HNO_3 also increases (equation (47)). Due to the high reactivities of NO and NO_2 , their densities are relatively small compared to products such as HNO_3 and N_2O . Most of the NO is lost by reduction to N_2 (equation (36)) and oxidation to NO_2 (equations (53) and (55)) and to a lesser degree to

HNO_2 (equation (54)). Most of the NO_2 is converted to HNO_3 (equation (47)). The end result of the increased production of NO and NO_2 is the increased density of HNO_3 and N_2O . N_2O_5 is mainly produced by the reaction of NO_2 with NO_3 (equation (60)) and so its production increases. This increase is offset by the increase in its unimolecular decomposition and so its density decreases.

The web speed and repetition rate of the discharge pulses determine the energy deposition and the time between generation of radicals. For example, as the web speed increases, the residence time of PP decreases and so the discharge frequency must be increased to keep the energy deposition constant (for a fixed voltage). Time-averaged and exit densities of gas phase species and concentrations of surface species are shown in figure 16 as a function of web speed for a constant energy deposition. As the pulse repetition frequency increases with web speed, O and OH radicals are refreshed more frequently, their time-averaged densities increase, and so their fluxes to the PP surface increase (figure 16(a)). Although the fluxes of O and OH increase with web speed, the surface concentrations of the alcohol, peroxy, carbonyl, and acid groups decrease (figure 16(b)). As the web speed increases from 150 to 350 cm s^{-1} , the residence time of the PP decreases from 0.08 to 0.03 s . Since the reactions on the PP surface that produce these groups occur on timescales on the order of a few tens of milliseconds, a factor of two change in the residence time noticeably affects their surface concentrations.

Although the densities of NO and NO_2 increase with the web speed (figure 16(c)), the change is not significant. Most of the NO is consumed to produce N_2 and NO_2 (equations (36), (53), and (55)) and most of the NO_2 is consumed by OH to produce HNO_3 (equation (47)). Since these reactions occur on timescales of less than 1 ms , the densities of NO , NO_2 and the products they form (HNO_3 , N_2O , N_2O_5) are not significantly affected by the change in the residence time (figures 16(c) and (d)). The density of O_3 slightly decreases due to the smaller time available for the reaction of O with O_2 to produce O_3 (equation (38)). Due to the decrease in the density of carbonyl groups with web speed, the production of CO_2 also decreases.

6. Concluding remarks

The gas phase and surface kinetics during the atmospheric pressure humid-air plasma processing of PP have been investigated. Using a pseudo-homogeneous global kinetics model, the consequences of process variables such as energy deposition, RH, web speed, and gas temperature on the surface properties of PP were investigated. Increasing energy deposition leads to an increased production of alcohol, carbonyl, acid, and peroxy radicals on the PP surface while increasing the gas phase production of O_3 and $N_x O_y$. Increasing the RH resulted in decreased production of O_3 . The surface concentrations of peroxy radicals increased with RH while those of alcohol, carbonyl, and acid groups decreased. Increasing the gas temperature decreased the surface concentrations of alcohol, carbonyl, and acid groups while the concentration of peroxy radicals increased. While keeping the energy deposition constant, increasing the web speed resulted in decreased concentrations of alcohols, peroxy radicals, carbonyl, and acid groups, indicating that residence time is an important process variable.

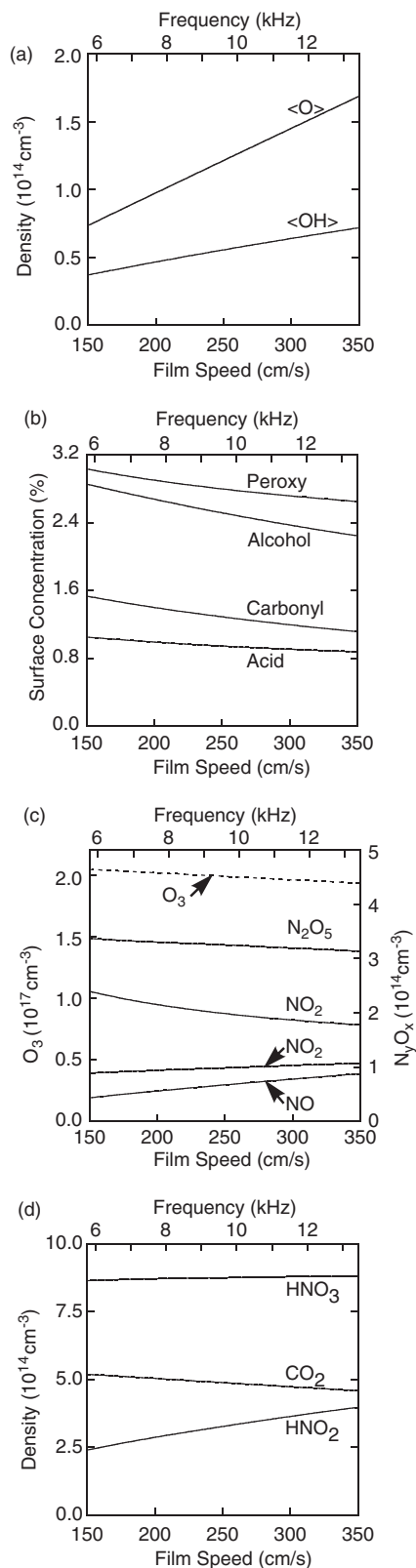


Figure 16. Exit surface properties of PP and time-averaged and exit densities of gas phase species as a function of web speed. (a) Time-averaged densities of O and OH (denoted as $\langle \text{O} \rangle$ and $\langle \text{OH} \rangle$). (b) Exit surface concentrations of alcohol, peroxy, carbonyl, and acid groups. (c) Exit O_3 and N_yO_x . (d) Exit CO_2 and HNO_x . To keep the energy deposition constant, the discharge frequency was adjusted. Conditions are otherwise the same as in figure 5.

Acknowledgments

This work was supported by the 3M Company and the National Science Foundation (CTS99-74962). The authors thank Dr Mark Strobel of the 3M Company for his valuable insights.

References

- [1] Chan C-M 1994 *Polymer Surface Modification and Characterization* 1st edn (New York: Hanser/Gardner)
- [2] Chan C-M, Ko T-M and Hiraoka H 1996 *Surf. Sci. Rep.* **24** 1
- [3] Zenkiewicz M 2001 *J. Adhesion Sci. Technol.* **15** 63
- [4] Strobel J M, Strobel M, Lyons C S, Dunatov C and Perron S J 1991 *J. Adhesion Sci. Technol.* **5** 119
- [5] Massines F and Gouda G 1998 *J. Phys. D: Appl. Phys.* **31** 3411
- [6] Poncin-Epaillard F, Chevet B and Brosse J-C 1994 *J. Adhesion Sci. Technol.* **8** 455
- [7] Shahidzadeh-Ahmadi N, Chehimi M M, Arefi-Khonsari F, Foulon-Belkacemi N, Amouroux J and Delamar M 1995 *Colloids Surf. A: Physicochem. Eng. Aspects* **105** 277
- [8] Strobel M, Dunatov C, Strobel J M, Lyons C S, Perron S J and Morgen M C 1989 *J. Adhesion Sci. Technol.* **3** 321
- [9] Strobel M, Lyons C S, Strobel J M and Kapaun R S 1992 *J. Adhesion Sci. Technol.* **6** 429
- [10] Clouet F and Shi M K 1992 *J. Appl. Polym. Sci.* **46** 1955
- [11] Foerch R, Kill G and Walzak M J 1993 *J. Adhesion Sci. Technol.* **7** 1077
- [12] Foldes E, Toth A, Kalman E, Fekete E and Tomasovszky-Bobak A 2000 *J. Appl. Polym. Sci.* **76** 1529
- [13] Lynch J B, Spence P D, Baker D E and Postlethwaite T A 1999 *J. Appl. Polym. Sci.* **71** 319
- [14] Takahashi N, Goldman A, Goldman M and Rault J 2000 *J. Electrostatics* **50** 49
- [15] Wells R K, Badyal J P S, Drummond I W, Robinson K S and Street F J 1993 *J. Adhesion Sci. Technol.* **7** 1129
- [16] Ishikawa S, Yukimura K, Matsunaga K and Maruyama T 2000 *Japan. J. Appl. Phys.* **39** 5223
- [17] Egitto F D, Matienzo L J, Blackwell K J and Knoll A R 1994 *J. Adhesion Sci. Technol.* **8** 411
- [18] Seeböck R, Esrom H, Charbonnier M and Romand M 2000 *Plasmas Polym.* **5** 103
- [19] Hofrichter A, Bulkin P and Drevillon B 2002 *J. Vac. Sci. Technol. A* **20** 245
- [20] Biederman H, Slavinska D, Boldyreva H, Lehmborg H, Takaoko G, Matsuo J, Kinpara H and Zemek J 2001 *J. Vac. Sci. Technol. B* **19** 2050
- [21] Shenton M J, Lovell-Hoare M C and Stevens G C 2001 *J. Phys. D: Appl. Phys.* **34** 2754
- [22] Guimond S, Radu I, Czeremuszkina G, Carlsson D J and Wertheimer M R 2002 *Plasmas Polym.* **7** 71
- [23] Wettermann R P 1990 *Medical Device and Diagnostic Industry*, vol 76
- [24] Kaelble D H 1970 *J. Adhesion* **2** 66
- [25] O'Hare L-A, Leadley S and Parbhoo B 2002 *Surf. Interface Anal.* **33** 335
- [26] Gheorghiu M, Arefi F, Amouroux J, Placinta G, Popa G and Tatouliau M 1997 *Plasma Sources Sci. Technol.* **6** 8
- [27] Hansen R H, Pascale J V, De Benedictis R and Rentzepis P M 1965 *J. Polym. Sci.: Part A: Polym. Chem.* **3** 2205
- [28] Poncin-Epaillard F and Aouinti M 2002 *Plasmas Polym.* **7** 1
- [29] Poncin-Epaillard F, Brosse J C and Falher T 1999 *Macromol. Chem. Phys.* **200** 989
- [30] Boyd R D, Kenwright A M, Badyal J P S and Briggs D 1997 *Macromolecules* **30** 5429
- [31] Strobel M and Lyons C S 2003 *J. Adhesion Sci. Technol.* **17** 15
- [32] Mukhopadhyay S, Joshi P, Datta S, Zhao J and France P 2002 *J. Phys. D: Appl. Phys.* **35** 1927
- [33] Hegemann D, Brunner H and Oehr C 2002 *Plasmas Polym.* **6** 221

- [34] Shahidzadeh N, Arefi-Khonsari F, Chehimi M M and Amouroux J 1996 *Surf. Sci.* **352–354** 888
- [35] Massines F, Gouda G, Gherardi N, Duran M and Croquesel E 2001 *Plasmas Polym.* **6** 35
- [36] Meiners S, Salge J G H, Prinz E and Forster F 1998 *Surf. Coat. Technol.* **98** 1121
- [37] Dorai R and Kushner M J 2002 *J. Phys. D: Appl. Phys.* **35** 2954
- [38] Dorai R 2002 *PhD Thesis* (Chemical and Biomolecular Engineering) University of Illinois <<http://uigelz.ecce.uiuc.edu/theses.html>>
- [39] Rockwood S D 1973 *Phys. Rev. A* **8** 2348
- [40] Bird R B, Stewart W E and Lightfoot E N 1994 *Transport Phenomena* 1st edn (Singapore: Wiley)
- [41] Brown P N, Hindmarsh A and Byrne G D 1998 VODE—Variable-coefficient ordinary differential equation solver
- [42] Piper L G 1987 *J. Chem. Phys.* **87** 1625
- [43] Atkinson R, Baulch D L, Cox R A, Hampson R F Jr, Kerr J A, Rossi M J and Troe J 1997 *J. Phys. Chem. Ref. Data* **26** 521
- [44] Atkinson R, Baulch D L, Cox R A, Hampson R F Jr, Kerr J A, Rossi M J and Troe J 1997 *J. Phys. Chem. Ref. Data* **26** 1329
- [45] Person J C and Ham D O 1988 *Radiat. Phys. Chem.* **31** 1
- [46] Ikezoe Y, Matsuoka S, Takebe M and Viggiano A 1987 Gas phase ion–molecule reaction rate constants through 1986 (Tokyo: Ion Reaction Research Group of The Mass Spectroscopy Society of Japan)
- [47] Atkinson R, Baulch D L, Cox R A, Hampson R F Jr, Kerr J A and Troe J 1989 *J. Phys. Chem. Ref. Data* **18** 881
- [48] Mirokin Y and Mallard G 1998 The NIST Chemical Kinetics Database
- [49] Tsang W and Hampson R F Jr 1986 *J. Phys. Chem. Ref. Data* **15** 1087
- [50] Mukkavilli S, Lee C K, Varghese K and Tavlarides L L 1988 *Trans. Plasma Sci.* **16** 652
- [51] Baulch D L *et al* 1994 *J. Phys. Chem. Ref. Data* **23** 847
- [52] Atkinson R 1997 *J. Phys. Chem. Ref. Data* **26** 215
- [53] Tsang W and Herron J T 1991 *J. Phys. Chem. Ref. Data* **20** 609
- [54] Carlsson D J and Wiles D M 1976 *J. Macromol. Sci.-Rev. Macromol. Chem.* **C14** 65
- [55] Razumovskii S D, Kefeli A A and Zaikov G E 1971 *Eur. Polym. J.* **7** 275
- [56] Strobel M, Branch M C, Ulsh M, Kapaun R S, Kirk S and Lyons C S 1996 *J. Adhesion Sci. Technol.* **10** 515
- [57] Rabek J F 1995 *Polymer Photodegradation: Mechanisms and Experimental Methods* 1st edn (London: Chapman and Hall)
- [58] Niki E, Decker C and Mayo F R 1973 *J. Polym. Sci.: Polym. Chem.* **11** 2813
- [59] Gomez S, Steen P G and Graham W G 2002 *Appl. Phys. Lett.* **81** 19
- [60] Kuzuya M, Kondo S-i, Sugito M and Yamashiro T 1998 *Macromolecules* **31** 3230
- [61] Carlsson D J and Chmela S 1990 *Mechanisms of Polymer Degradation and Stabilization* 1st edn, ed G Scott (London: Elsevier Applied Science) p 329
- [62] Paltenghi R, Ogryzlo E A and Bayes K D 1984 *J. Phys. Chem.* **88** 2595
- [63] Wheale S H, Barker C P and Badyal J P S 1998 *Langmuir* **14** 6699
- [64] Decker C and Mayo F R 1973 *J. Polym. Sci.: Polym. Chem.* **11** 2847
- [65] Strobel M, Jones V, Lyons C S, Ulsh M, Kushner M J, Dorai R and Branch M C 2003 *Plasmas Polym.* at press
- [66] Shenton M J and Stevens G C 2001 *J. Phys. D* **34** 2761
- [67] Foulon-Belkacemi N, Goldman M, Goldman A and Amouroux J 1995 *IEE Proc.-Sci. Meas. Technol.* **142** 477
- [68] Mark H F 1981 *Encyclopedia of Chemical Technology* 3rd edn (New York: Wiley) p 689